

**UNCLASSIFIED**

---

---

**AD 274 325**

*Reproduced  
by the*

**ARMED SERVICES TECHNICAL INFORMATION AGENCY  
ARLINGTON HALL STATION  
ARLINGTON 12, VIRGINIA**



---

---

**UNCLASSIFIED**

NOTICE: When government or other drawings, specifications or other data are used for any purpose other than in connection with a definitely related government procurement operation, the U. S. Government thereby incurs no responsibility, nor any obligation whatsoever; and the fact that the Government may have formulated, furnished, or in any way supplied the said drawings, specifications, or other data is not to be regarded by implication or otherwise as in any manner licensing the holder or any other person or corporation, or conveying any rights or permission to manufacture, use or sell any patented invention that may in any way be related thereto.

2274325  
NASA TN D-1222



## TECHNICAL NOTE

D-1222

ELECTRODE CONFIGURATIONS FOR A WIND-TUNNEL HEATER  
INCORPORATING THE MAGNETICALLY SPUN ELECTRIC ARC

By Donald R. Boldman, Charles E. Shepard,  
and John C. Fakan

Lewis Research Center  
Cleveland, Ohio



NATIONAL AERONAUTICS AND SPACE ADMINISTRATION  
WASHINGTON

April 1962

NATIONAL AERONAUTICS AND SPACE ADMINISTRATION

---

---

TECHNICAL NOTE D-1222

---

ELECTRODE CONFIGURATIONS FOR A WIND-TUNNEL HEATER  
INCORPORATING THE MAGNETICALLY SPUN ELECTRIC ARCBy Donald R. Boldman, Charles E. Shepard,  
and John C. Fakan

## SUMMARY

Various arc heater configurations were tested over a range of nitrogen flow rates, power levels, and pressures. Results of an evaluation of an arc heater composed of a 0.75-inch thoriated-tungsten cathode, a cylindrical copper anode, and a magnetic-field coil are presented. A study to determine the independent effect of pressure on arc potential difference, heater efficiency, and stagnation enthalpy was conducted with this unit using a series of nozzles with throat diameters of 0.5, 0.25, and 0.125 inch. The arc potential difference was essentially independent of the pressure level except for any change in the operating mode. A change in the arc operating mode resulting in transition to a higher arc potential difference was observed between the flow rates of 0.0055 and 0.0075 pound per second using the 0.25-inch-throat-diameter nozzle. The highest values of stagnation enthalpy and arc heater efficiency were obtained at the conditions corresponding to the highest arc potential difference.

Results are also presented for a higher power heater composed of three 0.5-inch-diameter tungsten cathodes and the aforementioned anode with the magnetic-field coil. A plenum and a 0.5-inch-throat-diameter critical-flow nozzle were incorporated in this latter unit. A correlation of experimental values of stagnation enthalpy with the theoretical-equilibrium and frozen-flow values was attempted; however, the correlation was relatively poor because little was known about the actual flow process.

A simplified analysis of the effect of a nonuniform enthalpy profile on the theoretical average stagnation enthalpy shows qualitatively that a large discrepancy between experiment and theory can be expected if the temperature profile corresponds to a uniform hot core of gas surrounded by a much cooler region in which the ratio of the areas of the respective regions is equal to or approximately 1.

A comparison of the average stagnation enthalpy at the exit plane of the nozzle determined from total-pressure measurements with the value determined by an energy balance yielded results that agreed to within approximately 17 percent.

## INTRODUCTION

At the present time, there is a great need for large-scale high-temperature facilities capable of simulating the aerodynamic heating of blunt bodies during reentry. The Lewis Research Center is developing a facility in which an electric arc is to be used to provide the high stagnation enthalpies required to simulate the aerodynamic heating associated with reentry.

The problem of simulating flight conditions completely becomes rather complex in that it is difficult to simulate all flight phenomena simultaneously. For example, it is possible to reproduce the velocity or stagnation enthalpy and altitude spectrum in the laboratory, but Mach number simulation is often sacrificed. Fortunately, in studies of stagnation-point heat transfer to blunt bodies, the inability to simulate Mach number is relatively unimportant (ref. 1). Pressure distributions and, therefore, stagnation-point heat-transfer rates can be duplicated independent of the Mach number in the hypersonic regime (about Mach 3 or greater). Reynolds number simulation for such devices is not in a range of practical interest.

The velocity-altitude range that can be simulated depends primarily upon the stagnation enthalpy and the power density (the net power to the stream divided by the test-section area), provided that most of the thermal energy is converted into kinetic energy. Since the stagnation enthalpy will depend upon the net power and the mass-flow rate of the working fluid, the important parameters for an arc tunnel of a given cross-sectional testing area are the gross power of the electric arc, the heat losses to the various components, and the mass-flow rate.

The continuous heating of air or nitrogen to the desired stagnation conditions is primarily an electrode development problem. Carbon or graphite electrodes are employed in some of the present devices (refs. 2 and 3); however, the contamination of the gas stream and the chemical reactions that occur make these electrodes unsuitable for many applications. In a previous report (ref. 4), water-cooled metallic electrodes were described that yielded very low contamination rates. A magnetic field was employed to rotate the arc about the cylindrical anode. The use of a field to rotate the arc is beneficial in three ways: (1) The anode heat load is distributed over a large area so that high currents can be used without excessive vaporization of the anode material (low contamination rates), (2) the arc rotates rapidly so that the fluid is heated more uniformly, and (3) the potential drop in the gas is increased so that more power can be delivered to the stream at a given current. The main disadvantage is that rotational motion or swirl is introduced into the stream. Figure 1 depicts the magnetically spun electric arc discussed herein.

Although it is possible to develop working arc heaters by intuition and experiment, it is generally more advantageous to analyze such devices rigorously with the intent of attaining a better understanding of the physical phenomena occurring within the arc chamber. A thorough evaluation of an electrode configuration is necessary in order to determine optimum operating conditions and to provide insight for the design of higher power units.

This has been the theme of the electrode development program at the NASA Lewis Research Center, which is continuing with the following objectives:

- (1) Higher net power input and higher stagnation pressures for better flow simulation
- (2) Higher stagnation enthalpies
- (3) More uniform flow in addition to improved arc stability and low contamination rates

The immediate goal is the development of an arc heater that will deliver 1500 kilowatts to the gas stream at enthalpies ranging from 2000 to 12,500 Btu per pound. The program is primarily based on modifications of the magnetically spun arc of reference 4.

#### SYMBOLS

A	area
$d_t$	nozzle throat diameter
E	arc potential difference, v
$E_g$	generator potential difference, v
g	gravitational constant, 32.2 ft/sec <sup>2</sup>
H	enthalpy, Btu/lb
$\bar{H}_0$	stagnation enthalpy based on absolute zero reference temperature, $H_0 + \bar{H}_{0,i}$
$H_0^*$	stagnation enthalpy defined by eq. (A1)
$H_{0,i}$	room-temperature enthalpy, 130 Btu/lb
h	specific enthalpy, Btu/lb

I arc current, amp  
 J mechanical equivalent of heat, 778.2 ft-lb/Btu  
 K constant  
 $\dot{m}$  nitrogen mass-flow rate, lb/sec  
 P pressure, atm or lb/sq ft abs  
 $P_A$  power dissipated to anode, kw  
 $P_C$  power dissipated to cathode, kw  
 $P_G$  gross arc power, EI, kw  
 $P_N$  power dissipated to nozzle, kw  
 $P_P$  power dissipated to plenum, kw  
 p static pressure, atm or lb/sq ft abs  
 $R_b$  ballast resistance, ohms  
 r radius  
 $r_e$  nozzle exit radius  
 U gas velocity, ft/sec  
 W power converted to useful heating of gas, kw  
 $\eta$  arc heater efficiency, defined by eq. (1), percent  
 $\rho$  gas density, lb/cu ft

#### Subscripts:

c cold gas region  
 h hot gas region  
 s behind normal shock wave  
 0 stagnation conditions

#### Superscript:

- average

## DESIGN CONSIDERATIONS

In reference 4 it is shown that the 3/4-inch-diameter thoriated-tungsten cathode (1 percent thorium) limited the power input to the working fluid (nitrogen) when a water-cooled, cylindrical copper anode with magnetic rotation was used. This arrangement is shown in figure 2. Since the publication of reference 4, much time has been devoted to the development of better cathodes. The following designs were considered:

- (1) Graphite cathode
- (2) Argon-shielded (single) thoriated-tungsten rod
- (3) Water-cooled copper cylinder
- (4) Single thoriated-tungsten rod
- (5) Multiple (three) thoriated-tungsten rods

### Graphite Cathode

The graphite or carbon cathode can be used at very high power levels (megawatt range) and is currently used in several operating free-jet facilities. The contamination of the stream is relatively low; however, the presence of even small amounts of carbon or carbon compounds is undesirable in certain applications such as tests on combustible ablating materials (ref. 5).

### Argon-Shielded Cathode

The argon-shielded cathode incorporates an argon atmosphere about the thoriated-tungsten cathode and thus permits higher currents and/or operation at higher pressure levels than are possible in nitrogen. This work at the Lewis Research Center is in the preliminary stages, but initial results are encouraging. It appears possible to heat air directly by using only a few percent of argon (ref. 6). Figure 3 shows some of the designs presently being considered.

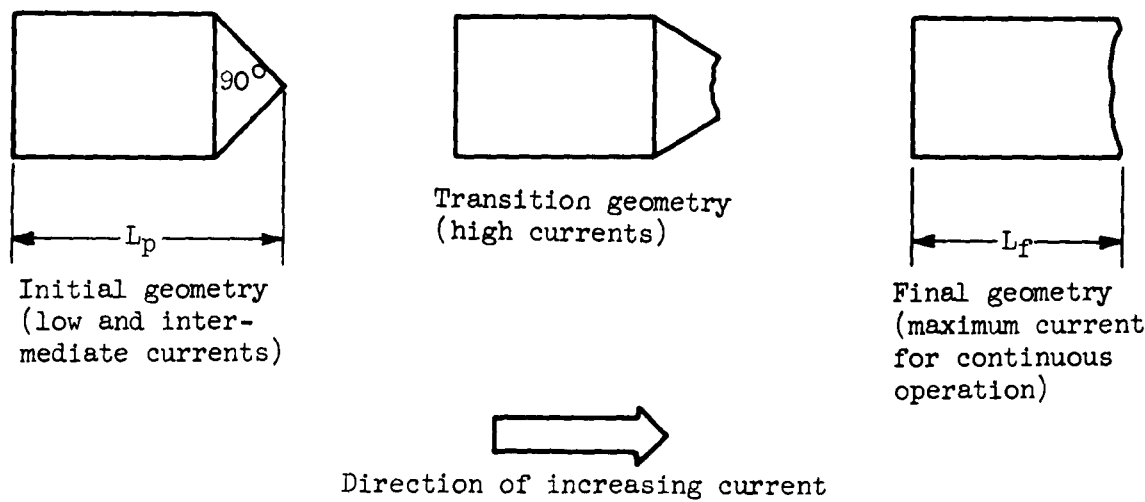
### Water-Cooled Copper Cathode

If the cathode is a water-cooled copper cylinder, both electrodes operate "cold." Therefore, gases that normally react with a hot cathode can be heated. Electrode emission from this type of cathode occurs by means other than thermionic emission (ref. 7). Alternating current can be used with this type of electrode configuration since either electrode

surface can act as the cathode (electron emitter). The power level of such a configuration can be quite high because both the cathode and anode spots are moved rapidly over their respective surfaces by the magnetic field. Operation at high pressures and moderate enthalpy levels is feasible with such devices. Two major problems that have been experienced with this type of concentric cylinder electrode configuration are longitudinal arc instability on the cathode and low efficiency. The problem of longitudinal instability can be avoided by the use of concentric water-cooled rings rather than cylinders. Successful arc units employing this geometry have been developed at the NASA Ames and Langley Research Centers and elsewhere.

#### Single Thoriated-Tungsten Cathode

The use of a single thoriated-tungsten rod as a cathode is discussed in detail in reference 4. There are several advantages peculiar to this type cathode. The arc becomes firmly attached to the pointed tip, as shown in figure 2, so that one end is fixed in space, and thus there is better control over the longitudinal position of the arc. At currents above a certain value, the pointed tip transforms to a blunt tip and finally to a nearly planar surface as shown in the following sequence of sketches:



The pointed tip has the additional advantage of being easier to start; however, the flat-faced tip can conduct a higher current. The cathode heat loss to the cooling water is low (about 5 percent of the power produced by the arc) compared with the losses of the water-cooled copper cylinder cathode of 20 to 25 percent (private communication with researchers at the NASA Langley Research Center). Lifetimes of several hours can be attained with the thoriated-tungsten-tipped cathodes if their respective current limits are not exceeded.

C-128

The current limit of the pointed and flat-faced cathodes is arbitrarily defined as the highest current attainable with essentially no change in  $L_p$  or  $L_f$  with testing time. The current limit of the 0.75-inch-diameter pointed thoriated-tungsten cathode is approximately 1000 amperes in nitrogen at pressures less than 5 atmospheres. The current limit for the flat-faced cathode is about 1200 amperes under the same conditions. Preliminary tests have indicated that increasing the diameter of the flat-faced-tip from 0.75 to 1 inch permits operation at about 1500 amperes with little contamination. Since the tungsten cathodes are current limited, higher power levels can be achieved by (1) using multiple cathodes and (2) combining several units with a common plenum (ref. 2).

#### Multiple Thoriated-Tungsten Cathodes

Three cathodes have been used in conjunction with a common anode in order to achieve higher power levels, as suggested previously. This is the basis of the design shown in figure 4, in which three 0.75-inch rods with thoriated-tungsten tips are used together with a 2.5-inch-inner-diameter water-cooled copper sleeve. Later versions consisted of the configuration shown in figure 5, and finally the 0.75-inch-diameter rods were replaced with 0.5-inch-diameter rods (fig. 6). All the cathode rods that have been described use a water-cooled copper support and a solid pointed tip. The earlier attempts to extend the cooling near the tip of the thoriated-tungsten slug have been abandoned because this cooling approach imposed a very large temperature gradient near the tip. The high gradient increased the cathode heat loss to the coolant and caused high thermal stresses with subsequent cracking of the tungsten. The present designs use a length  $L_p$  of 2 diameters and a cone angle of 90°.

#### Plenum

Since incandescent tungsten oxidizes quite rapidly in the presence of oxygen, nitrogen rather than air is heated in the arc chamber when the tungsten cathode is used. The plenum, shown in figure 7, serves as a mixing chamber for cold oxygen and hot nitrogen, and from it a mixture of gases equivalent to air can be obtained for expansion through the nozzle. Although the heat losses from the hot gas to the water-cooled plenum walls are significant, it is generally necessary to use a plenum in any arc tunnel to reduce the time and spatial temperature and velocity fluctuations.

#### INSTRUMENTATION

The observed data consisted of measurements of nitrogen flow rate, cooling-water flow rate, pressure, coolant temperature rise, arc potential

drop, and current. The coolant flow rates and temperature increases were used to determine the heat losses of the various components. A schematic layout of the instrumentation is shown in figure 8.

#### Flow Rates

Cooling-water flow rates were measured with turbine-type flow transducers, and the outputs were fed to a frequency meter and counter. The flow rate of the working fluid was determined by means of a calibrated orifice. The orifice differential pressure was measured with a conventional mercury manometer, and a calibrated 0-to-150-pound-per-square-inch test gage was used to obtain the orifice upstream pressure. In some of the tests, it was necessary to measure a secondary mass-flow rate (e.g., argon for the argon-shielded cathode). These flows were measured with a rotameter. The flow rates ranged from 0.001 to 0.007 pound per second for argon and from 0.005 to 0.03 pound per second for nitrogen and air.

#### Pressure

The stagnation pressure was measured at the downstream end of the plenum by a water-cooled annular section in all tests of the triple-cathode configuration. This ring, which was designed for the injection of oxygen into the plenum, yielded an average value of the pressure at the periphery. The stagnation pressure of the single-cathode unit was measured at the upstream end of the unit to reduce errors attributable to the vortex. Chamber pressures were read on a sensitive aneroid absolute pressure gage having a range of 0 to 200 inches of mercury.

Nozzle total pressures behind the normal shock were probed as a check of the stagnation enthalpy measurement. The 0.312-inch-diameter water-cooled total-pressure probe shown in figure 9 was scanned across the stream to obtain transverse pressure profiles. The cooling-water flow rate to the probe was 0.1 pound per second at a pressure of 60 pounds per square inch gage. The estimated heat absorption limit of the tip at these conditions was about 1000 Btu per second per square foot. Total pressures from the probe were read on either a 0-to-100-millimeter absolute-pressure gage or on a conventional mercury manometer.

Exhaust pressure was read on a Wallace and Tierman aneroid absolute-pressure gage (0 to 100 mm Hg).

#### RESULTS

In the performance evaluation to be discussed herein, three variables were independently controlled, namely, (1) the gross power input  $P_G$ ,

(2) the nitrogen mass-flow rate  $\dot{m}$ , and (3) the nozzle throat diameter  $d_t$ . These quantities necessarily introduce new variables such as the arc potential difference  $E$  and current  $I$  ( $EI = \Phi_G$ ), the stagnation pressure  $P_0$ , and the net power to the gas  $W$ . The data were cross-plotted so that the absolute variation of the important arc characteristics with the basic parameters could be determined.

138  
E

Since for a given mass-flow rate the plenum pressure is primarily a function of the nozzle throat diameter, the independent effect of stagnation pressure on arc heater performance can be obtained by using nozzles of various throat diameters. The number of nozzles required in an evaluation of this type depends upon the nature of the variation of the parameters with pressure. For instance, if maximums or minimums occur, the determination of these values may require the use of several nozzles.

Many data are generally required for a complete evaluation of an electrode configuration, and therefore long running times can be anticipated. A performance evaluation was conducted using nitrogen for the working fluid and an electrode configuration consisting of a single 0.75-inch-diameter thoriated-tungsten cathode and a 2.5-inch-diameter by 7-inch-long anode in conjunction with various sizes of converging-diverging nozzles (fig. 10). This configuration was selected because (1) the simplicity of design expedited disassembly for inspection of the electrodes and (2) the electrode geometry remains fixed (low contamination rates) for running times of several hours provided the current limit of the cathode is not exceeded.

The results of this evaluation are presented for three nozzles ( $d_t = 0.125, 0.25$ , and  $0.5$  in.) exhausting into the room. Results are also presented for the triple-cathode configuration in which a 0.5-inch-throat-diameter nozzle was used in conjunction with a plenum and test chamber (fig. 6) operating with an exhaust pressure of approximately 10 millimeters of mercury absolute. In all cases the data have been cross-plotted and presented in terms of common mass-flow rates. The stagnation pressure is related to the mass-flow rate and stagnation enthalpy as shown in figures 11 and 12 for a typical single-cathode configuration (0.25-in.-throat-diameter nozzle) and the triple-cathode configuration, respectively.

In all the tests with the single-cathode arc unit, the magnetic field was held constant at a strength of 1000 gauss in the center of the anode. This was achieved by exciting the coil with a 600-ampere direct-current welder generator. A systematic investigation of the effect of field strength on arc potential was not attempted; however, a few tests conducted with the single-cathode configuration, where the magnetic field was varied, have indicated a definite increase in arc potential drop with increasing field strength for given values of arc current, mass-flow rate,

and nozzle diameter. In tests with the triple-cathode unit, the field coil was excited in series with the electrodes, and therefore the field strength was proportional to the arc current.

#### Arc Potential Characteristics

In figures 13 and 14, the arc potential drop (all potential differences were measured with respect to the building ground) is plotted as a function of the arc current for various mass-flow rates. The operating potential difference is established by superimposing the supply (generator and ballast) load line, defined by

$$E = E_g - IR_b$$

(where  $R_b$  is considered part of the generator) upon the arc potential characteristic. Generally, for the data reported, the open circuit potential  $E_g$  is varied, and the ballast resistance  $R_b$  is held constant at 0.32 ohm for the single cathode and 0.16 ohm per cathode with 0.07 ohm external ballast for the triple cathodes. The intersection of the generator load line and the arc potential characteristic determines the stable operating point for the arc. This can be set by manipulating the open circuit potential and mass-flow rate.

Figures 13 and 14 indicate an increase in arc potential with increasing nitrogen flow rate and a decrease in potential with increasing current. Figure 13 is for the heater of figure 10, where a magnetic-flux density of 1000 gauss is maintained, and figure 14 is for the unit of figure 7, where the flux density is proportional to current. The effect of mass-flow rate on potential is shown in figure 15 for the data of figure 13 and for a current of 1000 amperes. If only the data for the 0.125- and 0.5-inch-diameter throats were considered, the arc potential would apparently be insensitive to pressure level. However, the 0.25-inch-nozzle data show that there has been a change in the arc mode between the flow rates of 0.0055 and 0.0075 pound per second. This was observed to be a region of unstable arc behavior; therefore, a smooth curve between these flow rates could not be obtained. The effect of the transition to a high potential mode can be noted in all succeeding performance curves as a jump in gross power. A similar transition occurred between flow rates of 0.0014 and 0.0018 pound per second for the unit of figure 7.

#### Arc Heater Efficiency

Since this report is primarily concerned with electrodes, the losses of the cathode, cathode chamber (water-cooled section that separates the

E-1385

anode and cathode shown in fig. 7), anode, plenum (if applicable), and nozzle will be considered separately. The cathode loss is small (of the order of 5 percent of the total arc power, ref. 4) for thoriated tungsten. The cathode chamber is exposed to radiation from the arc, and this heat loss may be of the same order of magnitude as that of the cathode. The cathode chamber can be shortened or eliminated in future designs of the arc heaters. The anode heat loss includes the usual product of anode sheath potential difference and the current in addition to the forced-convection loss of the heated gas. There is also radiation from the arc filaments to the cold wall, which is believed to be relatively small (ref. 8). A detailed analysis of these losses is beyond the scope of this report, but experimental results are presented that indicate how these losses vary with the basic operating parameters, pressure, arc power input, and gas flow rates. The component losses divided by the gross arc power are shown in figures 16 and 17 for the single cathode with the various nozzle sizes and for the triple cathode with the 0.5-inch-throat-diameter nozzle, respectively. The combined cathode and cathode chamber losses (indicated only as cathode loss in the figures) range from about 1 to 8 percent of the total power input. The loss appears to decrease slightly with increasing flow rates. In the case of the 0.125-inch nozzle and the triple-cathode configurations this decrease was not discernible because of scatter in the data. The loss was highest at the high pressure (0.125-in. nozzle), probably because of increased radiative heat transfer.

The fractional heat loss of the anode decreases with increasing flow rate and increases with increasing gross power input (fig. 16). This same trend was reported for the large arc heater of reference 2, in which the dominant heat-transfer mechanism was believed to be aerodynamic heating. If the heat-transfer equation for axial turbulent flow in a pipe is used for the range of power levels and flow rates discussed in this report, only about 25 percent of the anode heat loss is accountable. In order to obtain a better approximation of the forced-convection heat transfer, the anode loss must be analyzed on the basis of turbulent vortex pipe flow. In this type flow the heat-transfer rate depends on factors such as surface roughness, wall curvature, and mixing due to the density gradients arising in the complex flow field and on the conventional parameters for forced convection. A quantitative discussion of the theoretical heat transfer is beyond the scope of this report, but a qualitative estimate is in order. As indicated in reference 9, the heat-transfer coefficient in vortex flow can be four times as large as the heat-transfer coefficient at the same mass flow in purely axial flow. This would tend to support the hypothesis that a large fraction of the anode heat loss is due to aerodynamic heating.

The curves for the 0.25-inch throat have a very steep positive slope (fig. 16(b)); however, the losses are much lower at this pressure level. The transition to a higher potential mode of operation, mentioned

previously, is reflected as a large increase in the gross power between the flow rates of 0.0055 and 0.0075 pound per second. The high-pressure data ( $d_t = 0.125$  in.) are quite different in that the curves for anode loss are concave downward (fig. 16(c)). The anode loss at the high pressure was quite large (75 to 84 percent of the gross power).

The arc heater efficiency can be defined as the ratio of the power to the gas divided by the gross arc power. This can be expressed as

$$\eta = 100 \left( 1 - \frac{\theta_C + \theta_A}{\theta_G} \right) \quad (1)$$

The usual definition of arc heater efficiency includes the plenum and nozzle losses as well as the electrode losses. The geometry of the plenum and nozzles can have an appreciable effect on the efficiency; therefore, a true measure of the arc heating efficiency is obtained if these losses are not included. Arc heater efficiencies are plotted as a function of the arc power and nitrogen flow rate (figs. 18 and 19). The efficiency increased with increasing mass-flow rates but decreased with increasing power level except for the 0.125-inch-throat-diameter nozzle at high pressure. The efficiency reached a minimum for the high-pressure data using the single-cathode configuration. Figure 17 indicates that highest efficiencies (correspondingly highest stagnation enthalpies) for a given gross power were obtained with the 0.25-inch-throat-diameter nozzle.

#### Plenum and Nozzle Losses

There are additional losses that must be considered if the electric arc is to be used as a wind-tunnel heater. The heat loss in the plenum and nozzle will reduce the overall efficiency and stagnation enthalpy. The plenum was used only with the triple-cathode configuration. The plenum and nozzle fractional heat losses, presented in figures 16 and 17, depend largely on configuration. Although the effectiveness of the plenum has not been established, visual observation of the flow indicates that a plenum is necessary to provide time for the decay of vorticity effects arising from the magnetically driven arc. If in addition multiple arc heads are considered for high-power operation, a plenum is required in order to manifold the individual heaters. Plenum losses varied from 10 to 20 percent of the power input. Nozzle losses were generally less than 10 percent of the gross power input. This illustrates that, in order to improve the performance, emphasis should be directed toward minimizing the anode loss. Plenum and nozzle losses, although significant, are not formidable.

### Stagnation Enthalpy

There has been some concern regarding the losses that should be considered in the determination of stagnation enthalpy. This problem arises in a correlation of the stagnation enthalpy determined by the energy-balance method with the enthalpy calculated from critical-flow theory. Such a correlation is discussed in the next section. To avoid confusion, the stagnation enthalpy discussed herein will be defined as follows:

E-1385

$$H_0 = \frac{\mathcal{G}_G - (\mathcal{G}_C + \mathcal{G}_A + \mathcal{G}_P)}{1.054 \dot{m}}$$

The value  $H_0$  actually represents the change in the enthalpy of the system and is the effective  $H_0$  at the entrance plane of the nozzle. The nozzle loss has been completely excluded along with the initial enthalpy (approx. 130 Btu/lb). The stagnation enthalpy is plotted as a function of the gross power and mass-flow rate in figures 20 and 21. The highest values of stagnation enthalpy obtained were 17,600 Btu per pound for the single-cathode configuration using a 1/4-inch-throat-diameter nozzle with a nitrogen flow rate of 0.004 pound per second and about 8100 Btu per pound for the triple-cathode unit with a flow rate of 0.008 pound per second. An interesting point to note is the apparent maximum in all the enthalpy curves with the exception of those for the 0.125-inch-throat-diameter nozzle. This is especially pronounced in the curves for the 0.25-inch-throat-diameter nozzle with the single-cathode configuration and also in those for the triple-cathode configuration. The envelope of the curves also appears to maximize at the maximum attainable stagnation enthalpy for the given electrode configuration and mode of operation. Unpublished data from the single- and triple-cathode configurations indicate that higher values of stagnation enthalpy can be obtained when high mass-flow rates are used (ranging from 0.02 to 0.03 lb/sec). The arc apparently changes operating modes at high flow rates, and the resulting transition to a higher arc potential is accompanied by a decrease in arc current. This higher potential mode of operation was the more efficient mode, but the arc was generally more unstable.

### Correlation of Data Using Calculated Equilibrium

#### and Frozen Critical (Choked) Nozzle Flow

An attempt was made to verify the experimentally determined stagnation enthalpy  $H_0$  by calculating the theoretical value corresponding to the measured mass-flow rate and stagnation pressure. Equilibrium- and frozen-nozzle-flow theories are considered in which the arc-heated

E-1385

nitrogen is assumed to be in thermodynamic equilibrium prior to the start of the expansion. Data from the triple-cathode configuration were used in the correlation because the flow more closely approximated the assumptions of one-dimensional, homogeneous, steady flow (resulting from the inclusion of a plenum). As stated previously, the measured enthalpy was determined by dividing the net power to the gas (excluding the nozzle loss) by the mass-flow rate. The charts of reference 10 were used to predict the stagnation enthalpy for the equilibrium case in which an isentropic expansion from stagnation to throat conditions was assumed in addition to the aforementioned conditions. Frozen-flow calculations were based on the information of reference 8, where the gas is assumed to freeze at the stagnation conditions upon expanding through the nozzle. References 8 and 10 present the thermodynamic properties of air rather than nitrogen; however, comparison of the critical-flow charts for air with those derived from the data of reference 11 for nitrogen indicated that little error is introduced in the analysis by using the air charts.

The results of the correlation are presented in figure 22. The experimental stagnation enthalpy  $\bar{H}_0$  includes the initial room-temperature enthalpy (130 Btu/lb); that is,

$$\bar{H}_0 = H_0 + H_{0,i}$$

Nearly all the experimentally determined values of stagnation enthalpy were higher than predicted by either the equilibrium- or frozen-nozzle-flow theories. The variation of stagnation pressure with mass-flow rate and stagnation enthalpy indicated that the power balance value of stagnation enthalpy had surprisingly little effect upon the flow rate (figs. 11 and 12). This phenomenon, which appears to be attributable to uncertainties in the measurements, can be noted in figure 22, in which several values of experimental stagnation enthalpy occur for each value of mass-flow rate and stagnation pressure ( $d_t = 0.5$  in.). In addition, the values of stagnation enthalpy based on critical flow are nearly constant. The failure to match the values of stagnation enthalpy based on the power balance to the values calculated from critical-flow considerations has also been reported by others in arc facilities that were quite different from the one considered here (refs. 12 and 13).

The following factors can introduce errors in the correlation:

- (1) The gas in the plenum may not be in thermodynamic equilibrium.
- (2) Since the gas has a tangential component of velocity (which is induced by the arc rotation), the flow is not one-dimensional.

(3) The flow is not isentropic since heat is removed in the nozzle.

(4) The heating is not completely uniform because of the nature of the arc and therefore will also vary with time.

(5) The plenum pressure measurement is subject to error because of the swirl existing in the flow. A tangential component of velocity will always yield a pressure at the wall that is higher than the mass average.

(6) At high enthalpies the viscous losses are higher.

E-1385

It is hoped that this correlation can be discussed in greater detail in a future report. The effect of nonuniform heating and the determination of  $\bar{H}_0$  from total-pressure measurements have been considered and are discussed in appendixes A and B, respectively.

#### CONCLUSIONS

The performance characteristics for the single- and triple-cathode configurations were evaluated over a range of power levels and mass-flow rates. In addition, the single-cathode configuration was evaluated over a range of pressures that were independently controlled by using nozzles with different throat diameters. The triple-cathode unit had a higher power capacity because of the increased total cathode current capacity; however, the current capacity of the single cathode could be increased to some extent by using larger diameter tungsten tips.

A systematic study of the effect of field current (magnetic-field strength) on arc potential was not performed. In certain tests, however, the arc potential was found to increase with increasing field strength for fixed values of the other parameters.

The arc potential increases with increasing nitrogen mass-flow rate for a given nozzle throat diameter. The arc mode can change at certain pressure levels and flow rates and cause a transition to a higher or lower arc potential. In the present investigation, the highest arc potentials were obtained with the single-cathode configuration using a 0.25-inch-throat-diameter nozzle. The highest potentials were a result of a change in the operating mode that occurred between the flow rates of 0.0055 and 0.0075 pound per second. The highest values of arc heater efficiency and stagnation enthalpy were obtained at the conditions corresponding to the high potential operating mode.

An attempt was made to compare experimental values of stagnation enthalpy with corresponding theoretical values based on measured values of mass-flow rate and stagnation pressure for the assumptions of one-dimensional, homogeneous, steady, critical (choked) nozzle flow for the

equilibrium- and frozen-flow cases. The correlation was not very good; however, this might be expected since very little is known about the actual flow process. Although critical flow does exist, it is nonadiabatic and deviates from the steady flow of an ideal gas in many other ways. The experimental data showed a surprisingly small effect of the stagnation enthalpy on the flow rate; the flow rate was primarily a function of the throat size and pressure. This phenomenon is attributed to uncertainties in the measurements.

In summary, the following general conclusions can be made:

1. Using single or multiple cathodes, nitrogen can be efficiently heated over a wide range of stagnation enthalpies (as high as 17,500 Btu/lb) with the water-cooled cylindrical copper anode and magnetic rotation.
2. Higher power levels can be achieved by using several cathodes and a common anode. Also, it is expected that several units could be manifolded to a common plenum for applications requiring very high input powers.
3. There is a definite effect of pressure upon the arc potential characteristics and operating parameters of an arc unit. A careful evaluation, including the investigation of the pressure effect, is required in order to obtain the conditions for optimum performance of the unit.
4. The relatively high heat-transfer rate to the anode coolant suggests an investigation of the anode heat-transfer mechanisms associated with the cylindrical anode design and magnetically spun arc. Such a study could possibly provide a firm basis for the design of more efficient anodes.

Lewis Research Center  
National Aeronautics and Space Administration  
Cleveland, Ohio, January 18, 1962

## APPENDIX A

EVALUATION OF THE EFFECTS OF A NONUNIFORM ENTHALPY  
 PROFILE ON THE THEORETICAL AVERAGE STAGNATION  
 ENTHALPY BASED ON PERFECT GAS LAWS

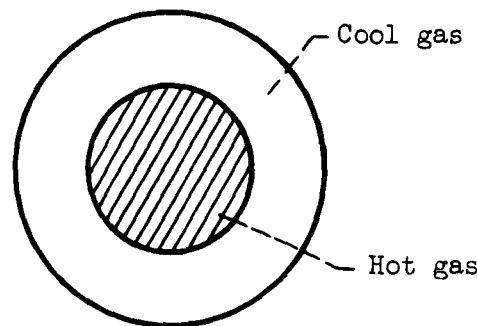
E-158

The use of a water-cooled nozzle in which the gas temperature at the wall is relatively low will introduce a test-section enthalpy profile with nonuniform characteristics.

The average stagnation enthalpy for a given enthalpy profile over an area  $A$  is given by

$$\bar{H}_0 = \frac{1}{A} \int_A H dA$$

In order to simplify the analysis an approximation of the physical case will be assumed in accordance with the following sketch:



With this model for the flow situation, it is desirable to compare the average stagnation enthalpy  $\bar{H}_0$  based on a nonuniform enthalpy profile with the theoretical-critical-flow value of stagnation enthalpy based on a uniform enthalpy profile  $H_0^*$ . In order to perform the evaluation, it is assumed that the fluid at the nozzle throat is divided into two regions, namely, a hot core of gas surrounded by a cool gas.

The following additional assumptions are made:

- (1) The pressure  $P_0$  is uniform across the plenum.

(2) An equation may be written

$$K_h = \frac{\dot{m}_h \sqrt{H_h}}{P_0 A_h} \quad \text{or} \quad K_c = \frac{\dot{m}_c \sqrt{H_c}}{P_0 A_c}$$

where  $K_h = K_c$  is applicable.

Of course, the assumption of a constant value of  $K$  is not completely correct since the hot core behaves as a real gas rather than a perfect gas. The value of  $K$  depends on the type of gas and the ratio of specific heats.

The net power to the gas is the sum of the net power to the cold and hot fluids; that is,

$$\begin{aligned} W &= \dot{m}_h H_h + \dot{m}_c H_c \\ &= W_h + W_c \end{aligned}$$

and  $A = A_h + A_c$ . The average stagnation enthalpy  $\bar{H}_0$  is simply the net power to the gas divided by the total mass-flow rate, or

$$\bar{H}_0 = \frac{W}{\dot{m}_h + \dot{m}_c} = \frac{\dot{m}_h H_h + \dot{m}_c H_c}{\dot{m}_h + \dot{m}_c}$$

Upon applying assumptions (1) and (2) and rearranging, the average stagnation enthalpy can be written in terms of the enthalpies and areas of the separate regions as

$$\bar{H}_0 = H_h \left( \frac{1 + \frac{A_c}{A_h} \sqrt{\frac{H_c}{H_h}}}{1 + \frac{A_c}{A_h} \sqrt{\frac{H_h}{H_c}}} \right)$$

If a theoretical value of enthalpy  $H_0^*$  is defined in accordance with assumption (2) as

$$H_0^* = \frac{K^2 P_0^2 A^2}{\dot{m}^2} \quad (\text{Al})$$

the average stagnation enthalpy  $\bar{H}_0$  determined from an energy balance will be equal to the theoretical value  $H_0^*$  divided by a factor that depends upon the values of  $A_h$ ,  $A_c$ ,  $H_h$ , and  $H_c$ . If the enthalpy profile is uniform,  $H_0^* = \bar{H}_0$ ; however, if the enthalpy profile is nonuniform according to the assumed model, the ratio  $H_0^*/\bar{H}_0$  can be determined as follows:

$$\frac{H_0^*}{\bar{H}_0} = \left( \frac{H_0^*}{H_h} \right) \left( \frac{H_h}{\bar{H}_0} \right)$$

$$H_h = \frac{K_h^2 P_0^2 A_h^2}{\dot{m}_h^2}$$

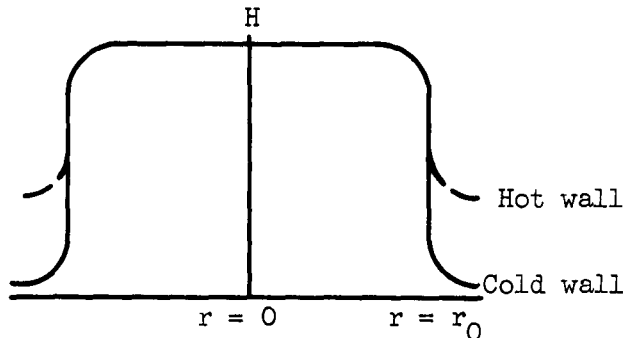
$$\frac{H_h}{H_0^*} = \frac{A_h^2 (\dot{m}_h + \dot{m}_c)^2}{A_c^2 \dot{m}_h^2}$$

$$\frac{H_0^*}{\bar{H}_0} = \frac{\left( \frac{A_c}{A_h} + 1 \right)^2}{\left( 1 + \frac{A_c}{A_h} \sqrt{\frac{H_c}{H_h}} \right) \left( 1 + \frac{A_c}{A_h} \sqrt{\frac{H_h}{H_c}} \right)} \quad (A2)$$

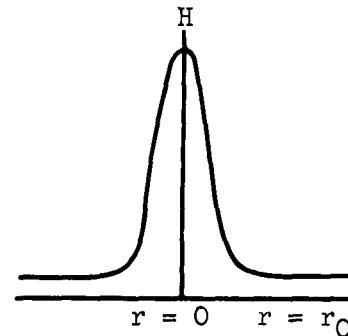
A graph of  $H_0^*/\bar{H}_0$  against  $A_c/A_h$  for various values of  $H_c/H_h$  is presented in figure 23. The quantitative use of equation (A2) is difficult since the hot and cold fluid regions are not clearly defined, but the relation indicates that a nonuniform enthalpy profile can adversely affect a correlation with theoretical values based on uniform properties, especially in the neighborhood of

$$\frac{A_c}{A_h} = 1$$

A good correlation should be expected if the enthalpy profile can be categorized by either of the two following cases:



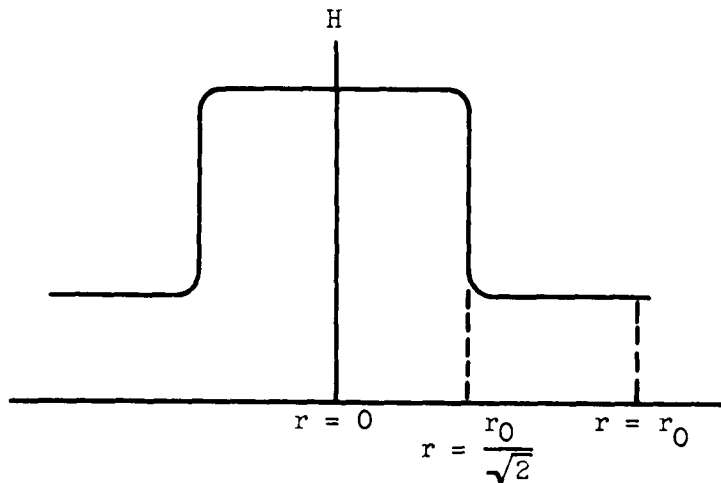
Case I.  $A_c/A_h \ll 1$ .



Case II.  $A_c/A_h \gg 1$ .

Case I represents the ideal uniform flow of a hot gas surrounded by a thin layer of cool gas (boundary layer). Such a flow might nearly be achieved by operating with a "hot" wall using a refractory type material. Case II represents the other extreme, in which a concentrated hot core exists.

The third case, for which a good correlation cannot be expected according to figure 23, consists of an enthalpy profile in which the areas of the hot and cold regions are approximately equal ( $A_c/A_h \approx 1$ ), as shown in the following sketch:



Case III.  $A_c/A_h = 1$ .

If this analysis is applied to a parabolic profile as indicated by the total-pressure profile of figure 24, it can be shown that a poor

correlation of experimental and theoretical values of stagnation enthalpy should be expected. (The total-pressure profile is related to the enthalpy profile, as discussed in appendix B.) For instance, if  $A_c/A_h = 1$  is considered for this case and the profile of figure 24 is approximated by

$$\left(\frac{r}{r_0}\right)^2 = -1.23\left(\frac{P_{0,s}}{P_0} - 0.52\right)$$

8  
1  
2  
3

integration over the areas  $A_h$  and  $A_c$  yields  $H_c/H_h = 0.017$ , corresponding to  $H_0^*/H_0 = 0.4$ .

## APPENDIX B

DETERMINATION OF THE AVERAGE STAGNATION ENTHALPY  
FROM TOTAL-PRESSURE MEASUREMENTS

The average velocity  $\bar{U}$  at the nozzle exit can be expressed as the integral of the momentum over the exit area divided by the total mass-flow rate:

$$\bar{U} = \frac{1}{\dot{m}} \int_A \rho U^2 dA$$

Since the pressure sensed by the probe  $P_{0,s}$  is approximately equal to the pressure behind the normal shock wave, the momentum equation for a normal shock wave is applicable; thus

$$P_{0,s} = p + \rho \frac{U^2}{g}$$

or

$$\bar{U} = \frac{2\pi g P_0 r_e^2}{\dot{m}} \left[ \int_0^1 \left( \frac{P_{0,s}}{P_0} \right) \left( \frac{r}{r_e} \right) d\left( \frac{r}{r_e} \right) - \int_0^1 \left( \frac{p}{P_0} \right) \left( \frac{r}{r_e} \right) d\left( \frac{r}{r_e} \right) \right] \quad (B1)$$

The average stagnation enthalpy is given by

$$\bar{H}_0 = \frac{\bar{U}^2}{2gJ} + h \quad (B2)$$

where adiabatic flow is assumed. The use of a cold wall nozzle induces a violation of this assumption that may be the greatest source of error in the method.

An approximation of the average stagnation enthalpy can be obtained if the values of  $p$  and  $h$  in equations (B1) and (B2) are considered to be much less than the corresponding stagnation values; that is, if  $p \ll P_0$  and  $h \ll H_0$ , the simplified equations become

$$\bar{U} = \frac{2\pi g P_0 r_e^2}{\dot{m}} \int_0^1 \left( \frac{P_{0,s}}{P_0} \right) \left( \frac{r}{r_e} \right) d\left( \frac{r}{r_e} \right) \quad (B1a)$$

and

$$\bar{H}_0 = \frac{\bar{U}^2}{2gJ} \quad (\text{B2a})$$

This is fully justified only if the expansion is ideally complete; that is, if all the thermal energy is converted into kinetic energy. A typical pressure profile is shown in figure 24. The transverse pressure survey resulted in a slightly asymmetrical profile. Therefore, an average value for the integral was used to determine  $\bar{U}$ . In this approximation, calculations based on total-pressure measurements yielded  $H_0 = 2330$  Btu per pound. The corresponding value of stagnation enthalpy determined from an energy balance (accounting for the nozzle loss) was 2800 Btu per pound, a discrepancy of approximately 17 percent.

Of course the error in the determination of  $\bar{U}$  becomes large if the expansion deviates appreciably from the ideal case. It is, then, necessary to account for the amount of latent heat at the nozzle exit. For example, if the static pressure of equation (B1) is considered in the analysis, the measured value of exit static pressure (0.0071 atm assumed constant) reduces the value of  $\bar{U}$  from 10,800 to 10,250 feet per second; however, this reduction in velocity would not necessarily correspond to a reduction in  $\bar{H}_0$ . The inclusion of  $h$  in equation (B2) corresponding to  $p$  tends to restore  $\bar{H}_0$  to the value originally determined by neglecting these terms. Hence, the assumption of a complete expansion should not introduce a serious error.

In this investigation the determination of  $h$  was difficult because little was known about the actual flow process. The difficulty was enhanced because a good correlation of experiment and theory could not be attained.

#### REFERENCES

1. Palmer, George M.: A Study of the Overall Problems of the True-Temperature, Hypersonic Wind Tunnel Having Semi-Continuous Operation and the Preferred Methods of Solution. Rep. A-59-14, Purdue Univ., Aug. 1959.
2. Rose, P. H., Powers, W. E., and Hritzay, D.: The Large High Pressure Arc Plasma Generator: A Facility for Simulating Missile and Satellite Re-Entry. Res. Rep. 56, Avco Corp., June 1959.
3. McGregor, W. K., Ehrlich, J. J., and Dooley, M. T.: Performance of a D-C Arc-Excited Plasma Generator. TN-60-112, Arnold Eng. Dev. Center, Aug. 1960.

- E-1385
4. Shepard, Charles E., and Boldman, Donald R.: Preliminary Development of Electrodes for an Electric-Arc Wind Tunnel. NASA MEMO 4-14-59E, 1959.
  5. Georgiev, S., and Rose, P. H.: On Carbon Contamination of Air Arcs and Its Effect of Ablation Measurements. Res. Note 177, Avco Corp., Dec. 1959.
  6. Anon.: Development and Possible Applications of Plasma and Related High-Temperature Generation Devices. MAB-167-M, Materials Advisory Board, Aug. 30, 1960.
  7. Somerville, J. M.: The Electric Arc. John Wiley & Sons, Inc., 1959, pp. 58-60.
  8. Stalder, Jackson R., Goodwin, Frederick K., Ragent, Boris, and Noble, Charles E.: Aerodynamic Applications of Plasma Wind Tunnels. Rep. 18, Vidya, Inc., Dec. 1960.
  9. Kreith, Frank, and Margolis, David: Heat Transfer and Friction in Turbulent Vortex Flow. Appl. Sci. Res., sec. A, vol. VIII, 1959, pp. 457-473.
  10. Moeckel, W. E., and Weston, Kenneth C.: Composition and Thermodynamic Properties of Air in Chemical Equilibrium. NACA TN 4265, 1958.
  11. Kanter, I. E., Martinek, F., and Ghai, M. L.: High Temperature Heat Transfer from Gases to Cylinders and Nozzles. AFOSR TN 59-488, General Electric Co., Feb. 1959.
  12. Boobar, Murray G.: Arc-Plasma Tunnels - A Review of the Present State-of-the-Art. Rep. 44, Vidya, Inc., Mar. 31, 1961.
  13. Clark, R. H., et al.: Performance Characteristics of a Vortex Stabilized Plasma Generator Using Argon. Rep. 7292, McDonnell Aircraft Corp., Feb. 1960.

E-1385

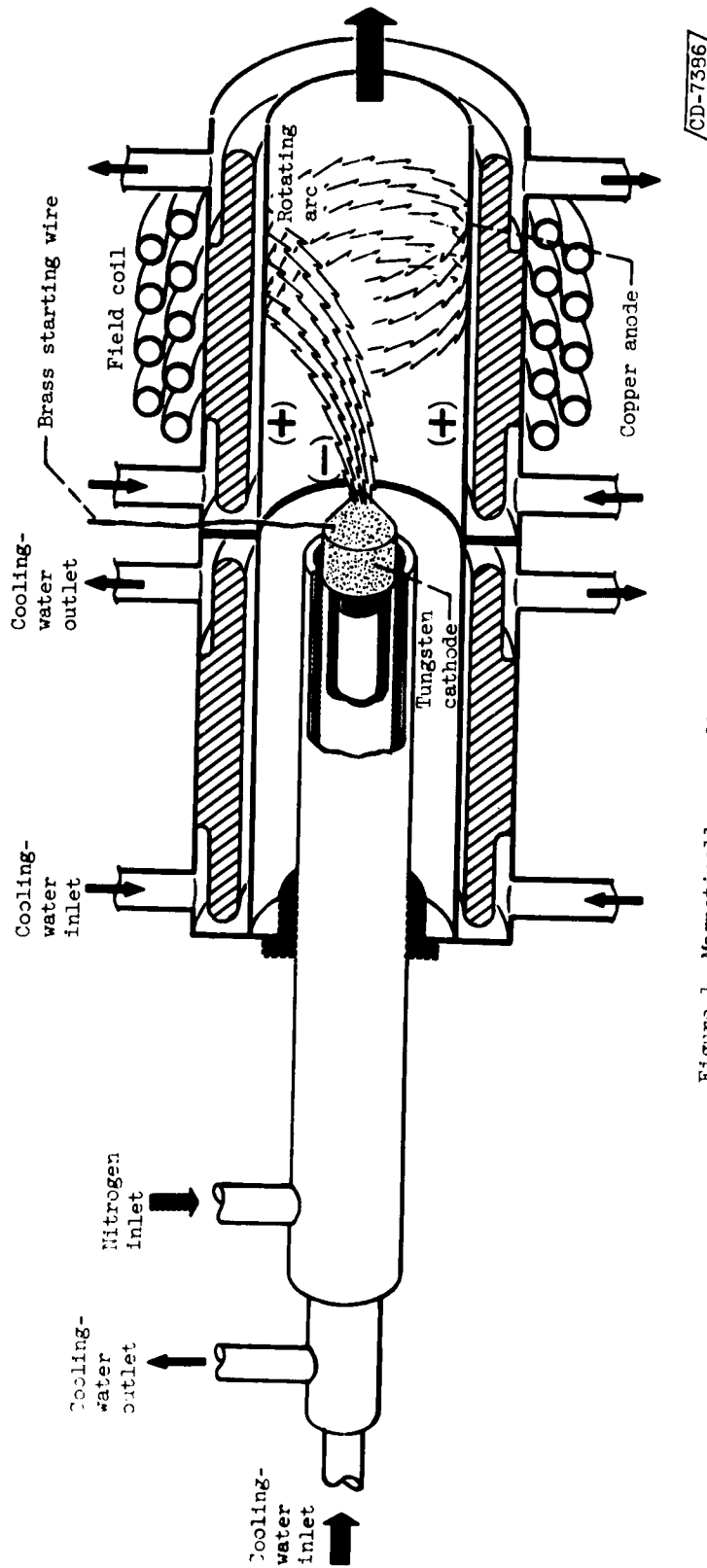


Figure 1. Magnetically span direct-current arc.

/CD-7336/

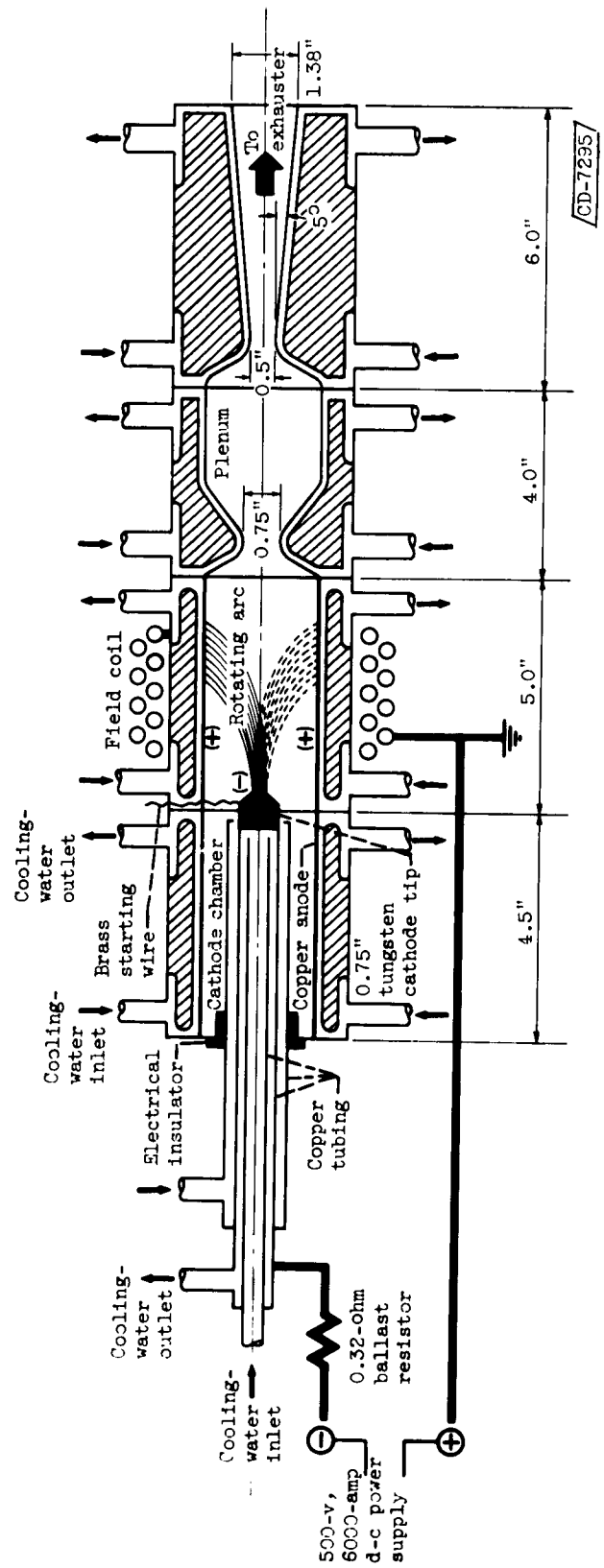
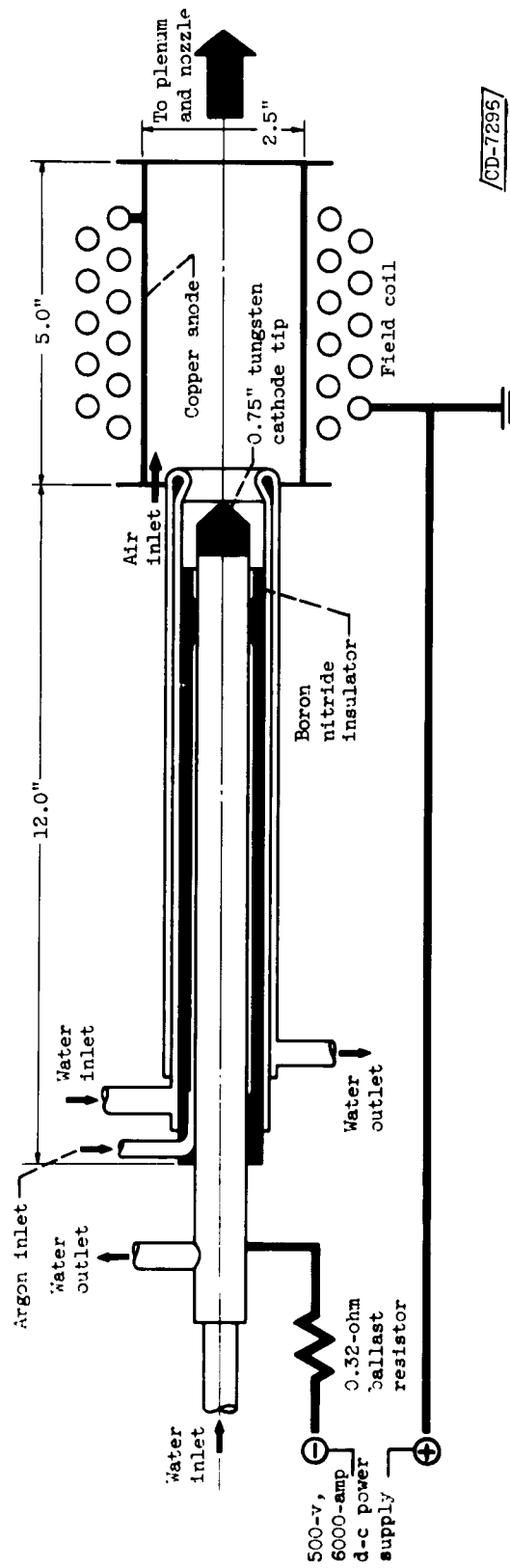


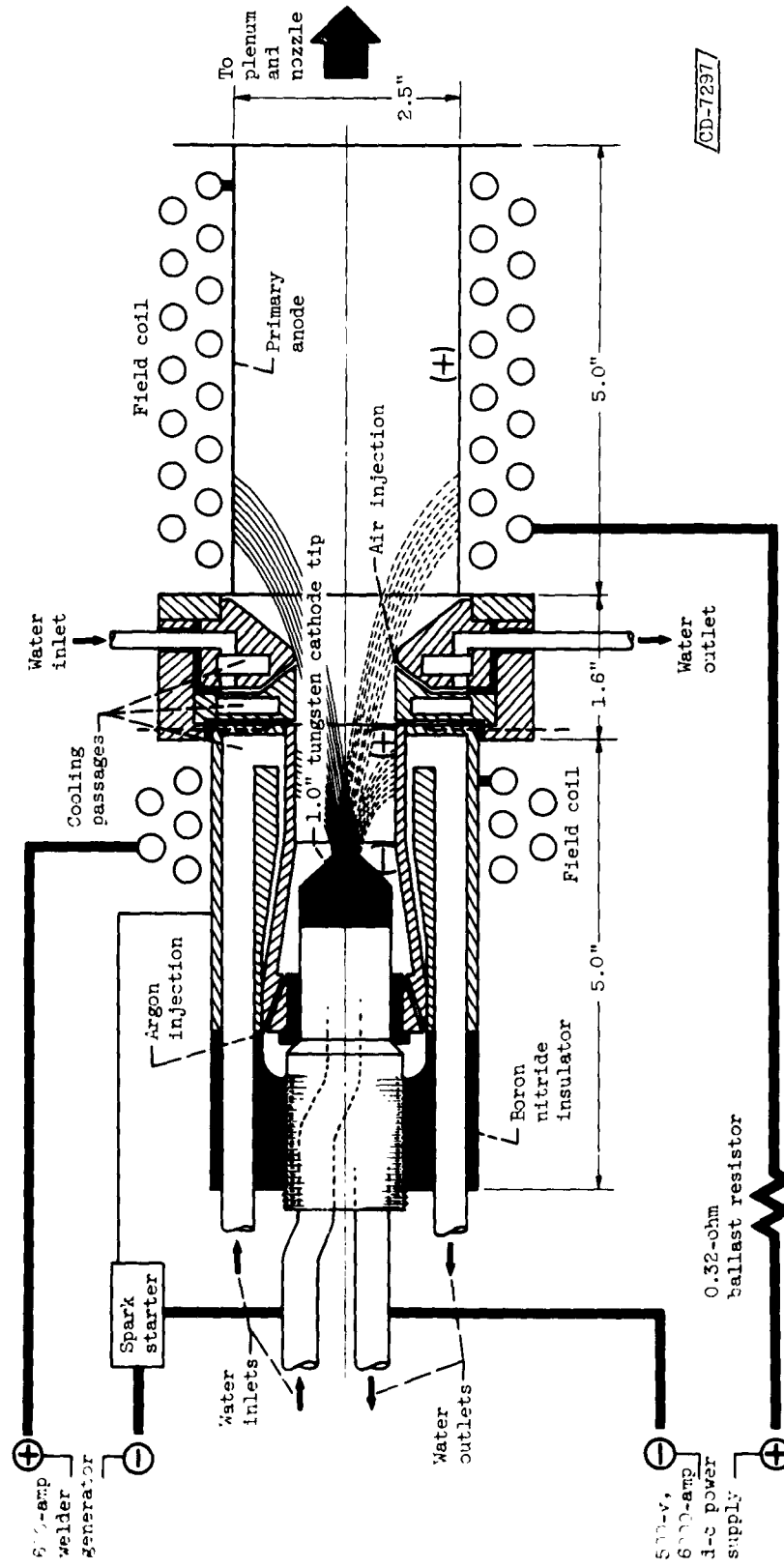
Figure 2. - Original electrode configuration (ref. 1) consisting of tungsten-tipped cathode, copper-sleeved anode, and magnetic-field coil.

E-1385



(a) 0.75-inch cathode with single anode.

Figure 3. - Argon-shielded-cathode configurations.



(b) 1-inch cathode with double anode.

Figure 3. - Concluded. Argon-shielded-cathode configurations.

E-1385

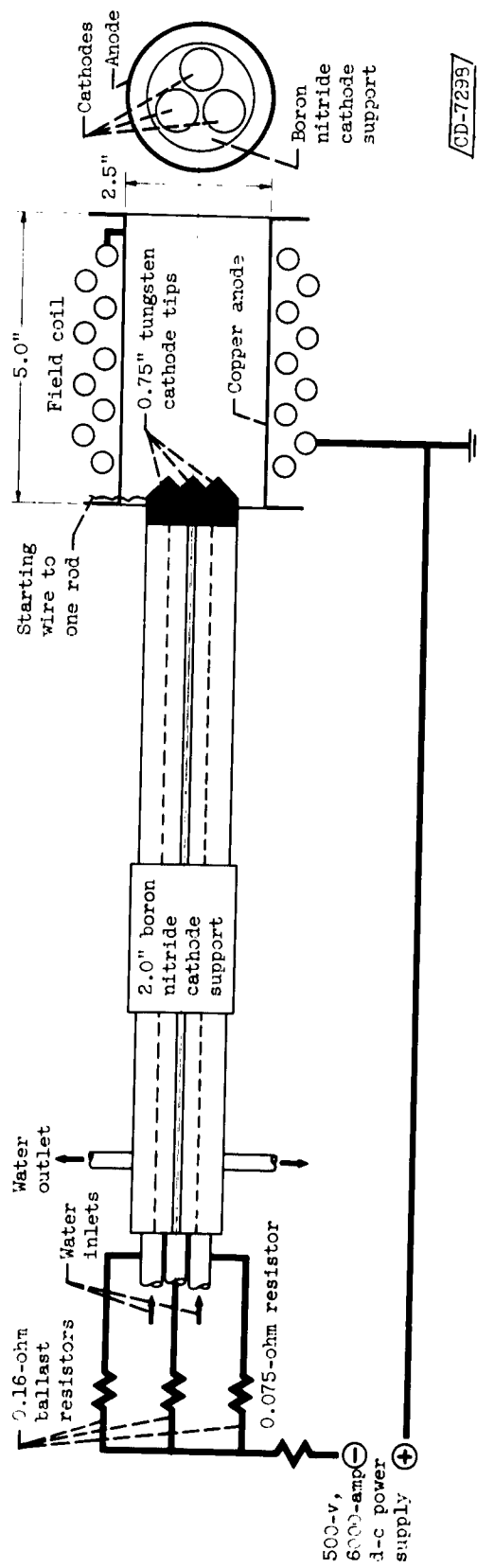


Figure 4. - Original triple-cathode configuration using three parallel 0.75-inch cathode rods.

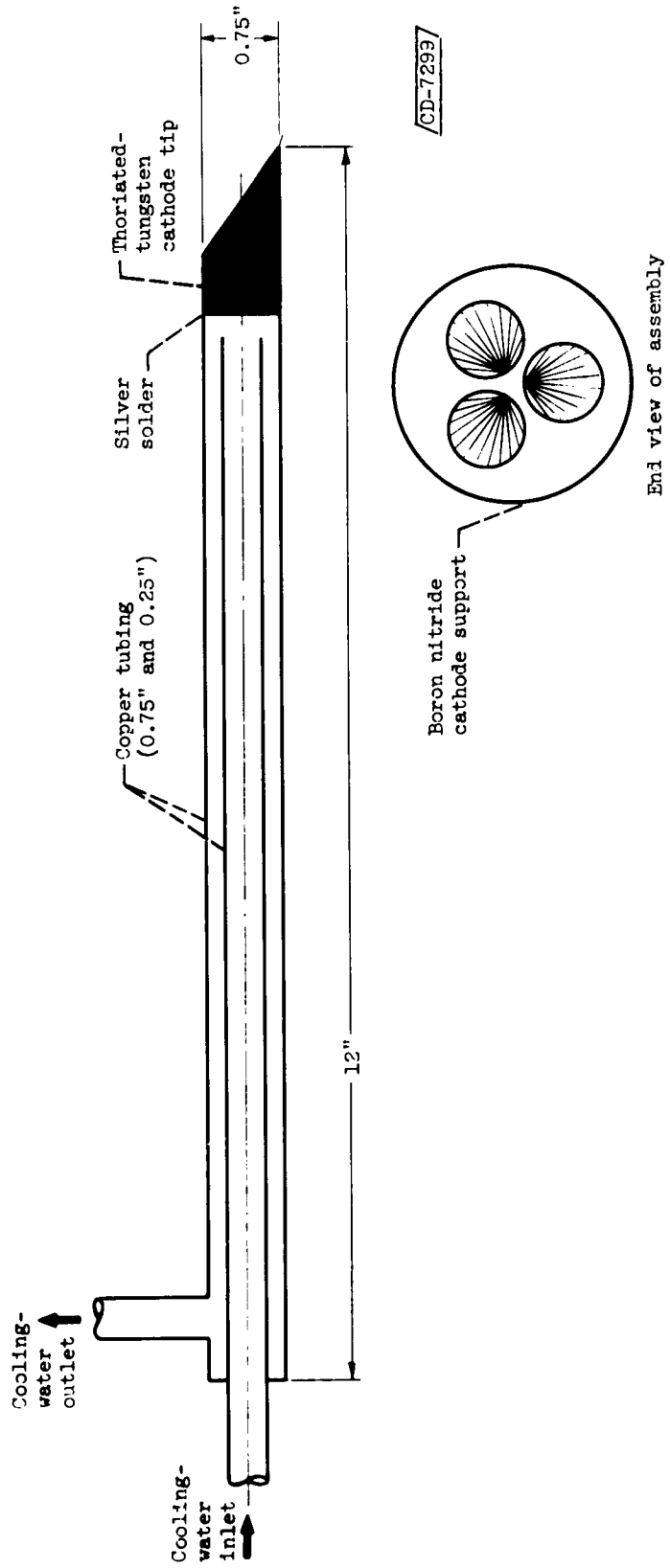


Figure 5. - Modified 0.75-inch cathode for multiple-cathode configuration.

E-1385

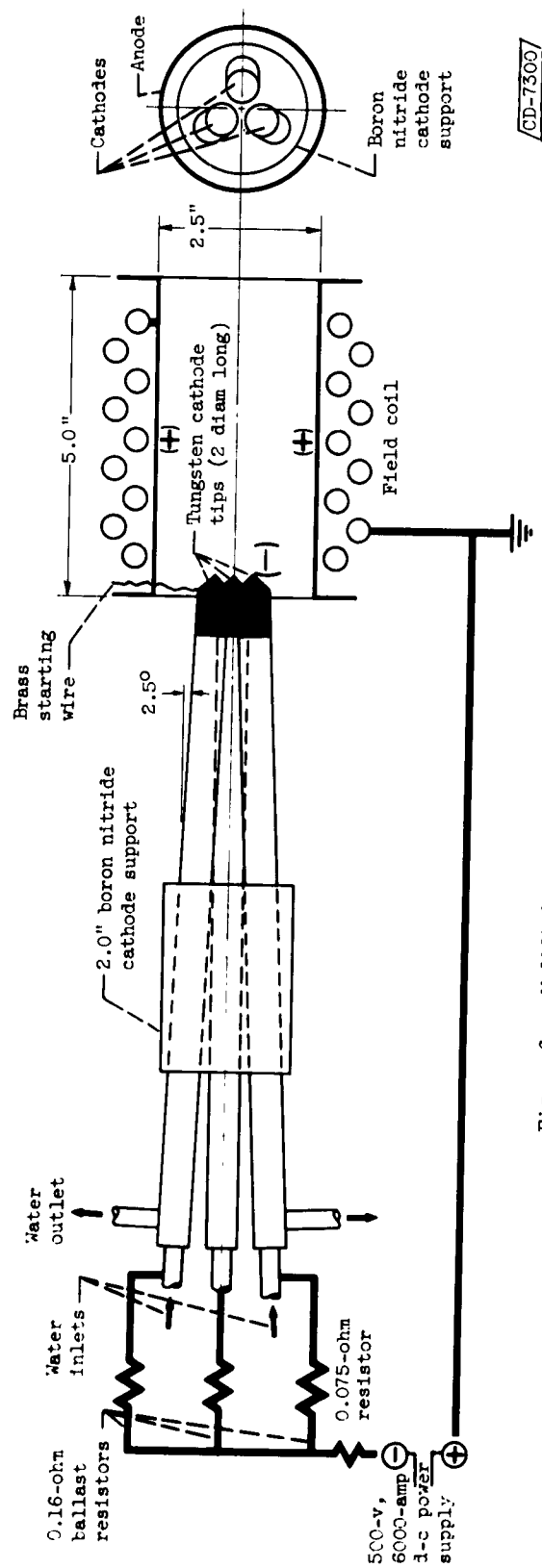


Figure 6. - Modified converging triple-cathode configuration.

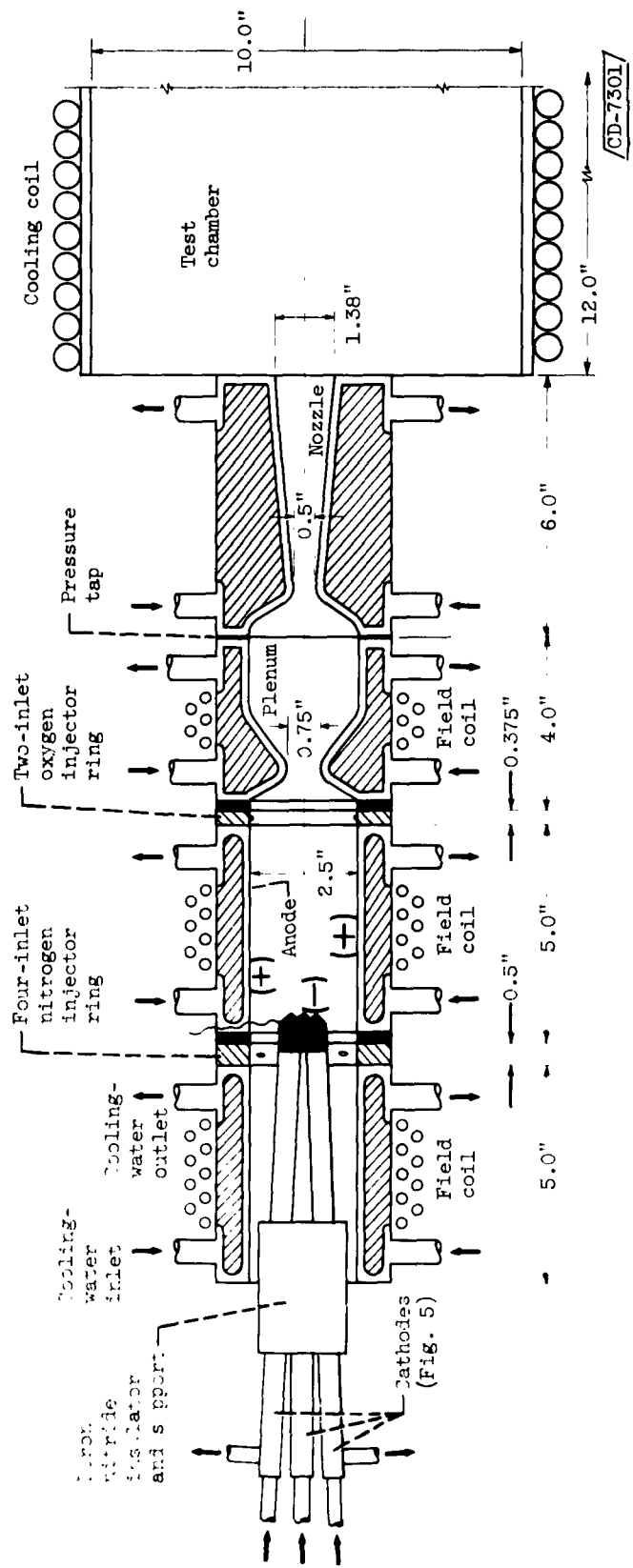


Figure 7. - Arc tunnel with electrode configuration of figure 5. Power, 200 kilowatts.

CRT-F

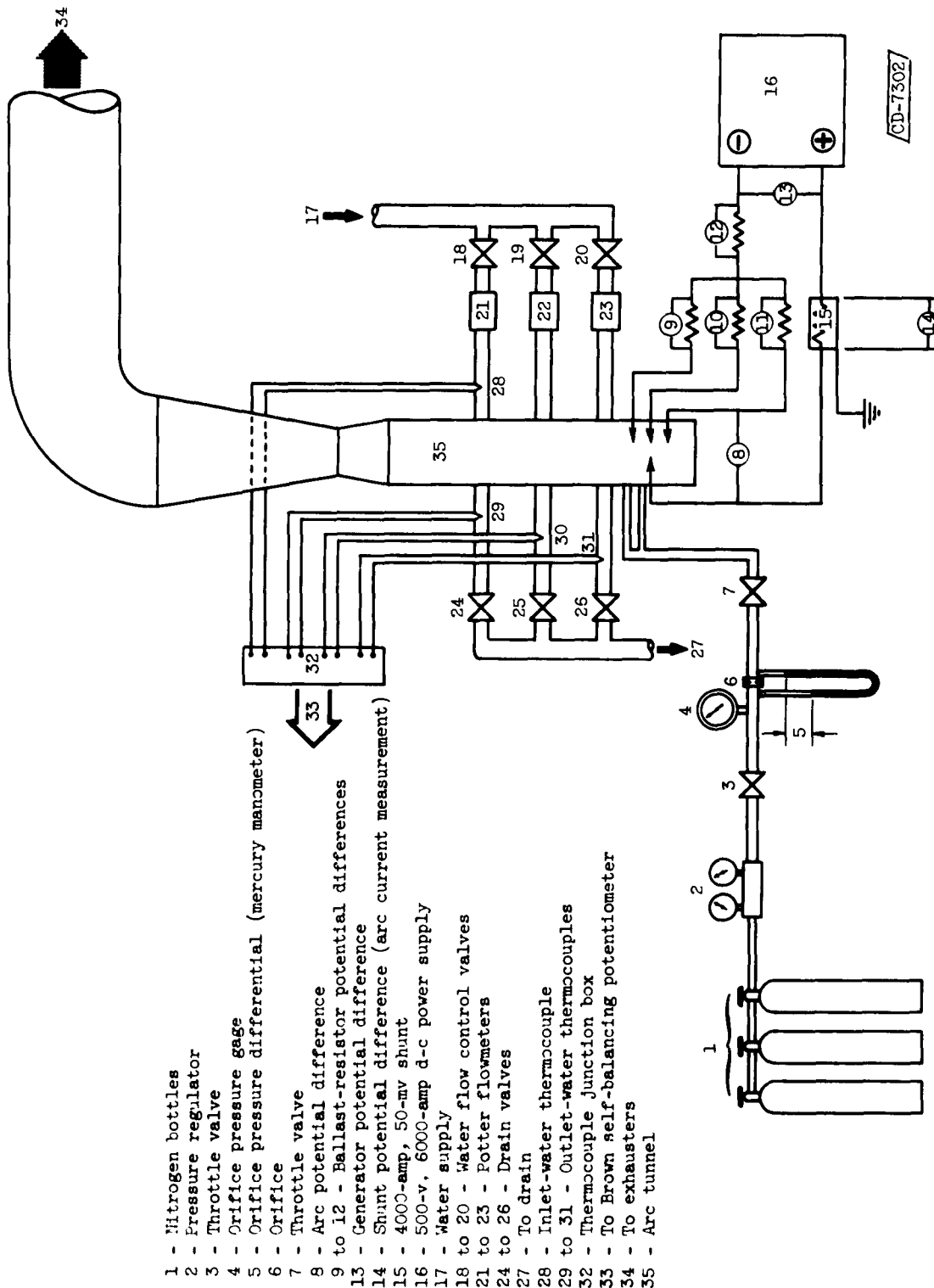


Figure 8. - Schematic diagram of instrumentation for 200-kilowatt arc tunnel.

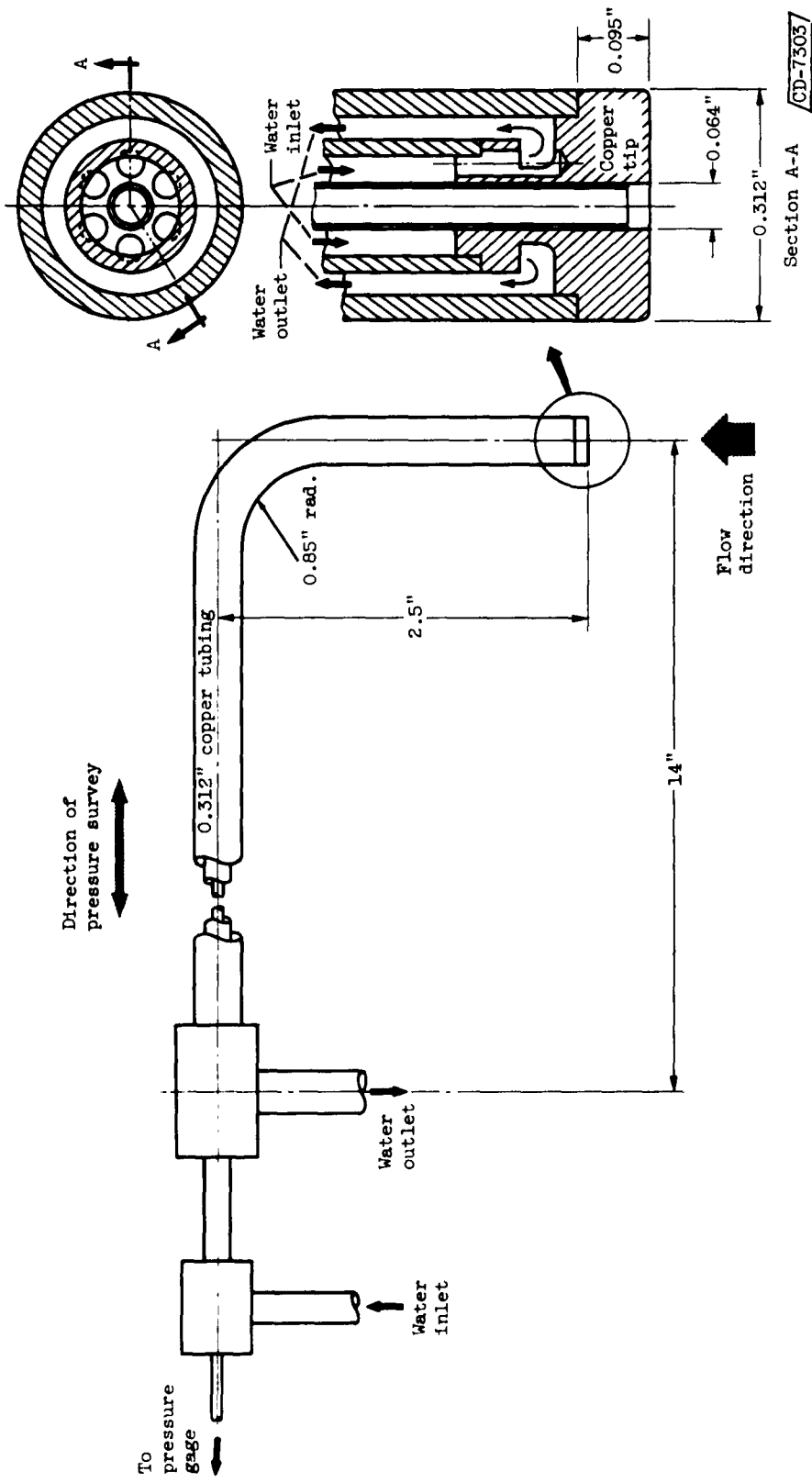


Figure 9. - Water-cooled total-pressure probe.

E-1385

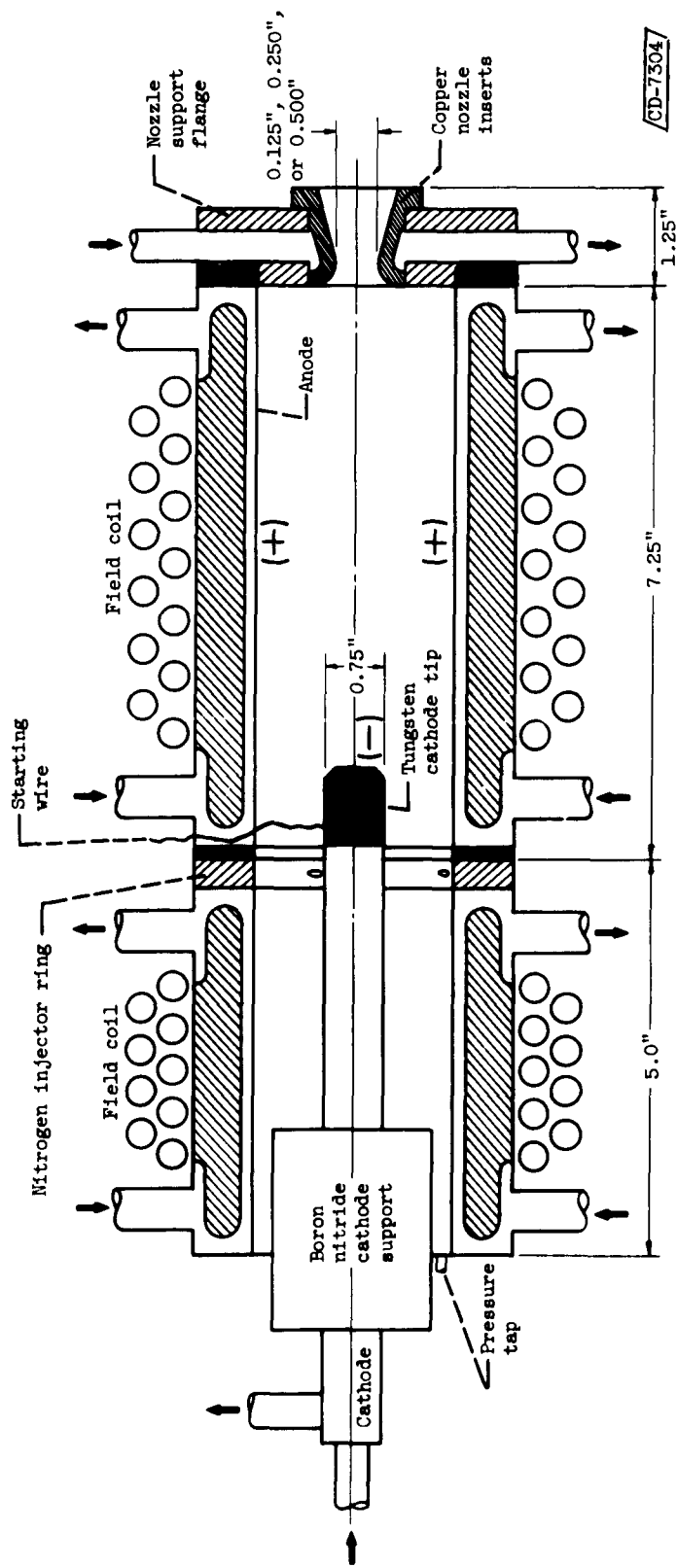


Figure 10. - Arc unit for study of effects of pressure on operating parameters.

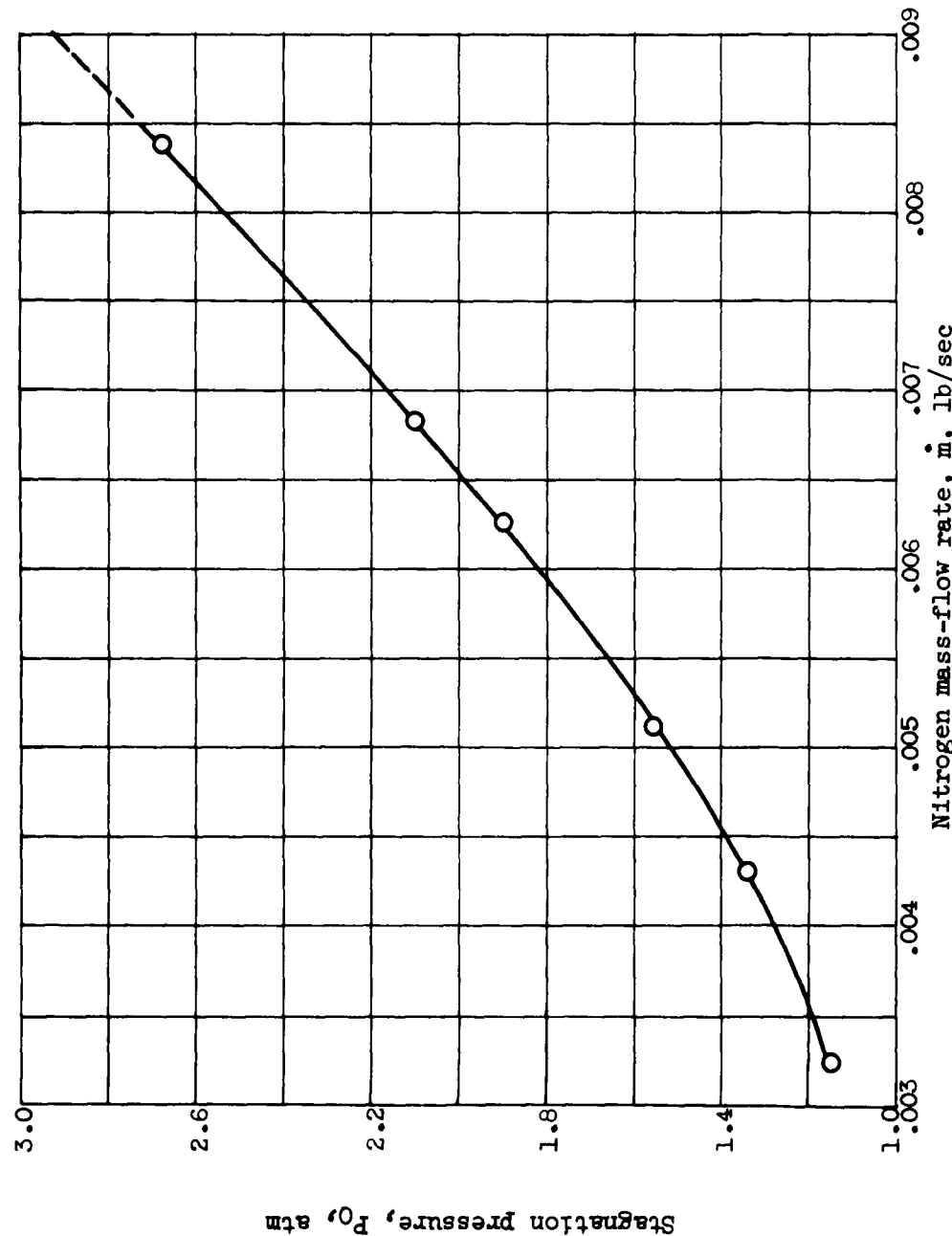


Figure 11. - Variation of stagnation pressure with nitrogen flow rate for single-cathode configuration using 0.25-inch-throat-diameter nozzle. Ballast resistor, 0.32 ohm; stagnation enthalpy, 11,000 to 17,500 Btu per pound.

E-1385

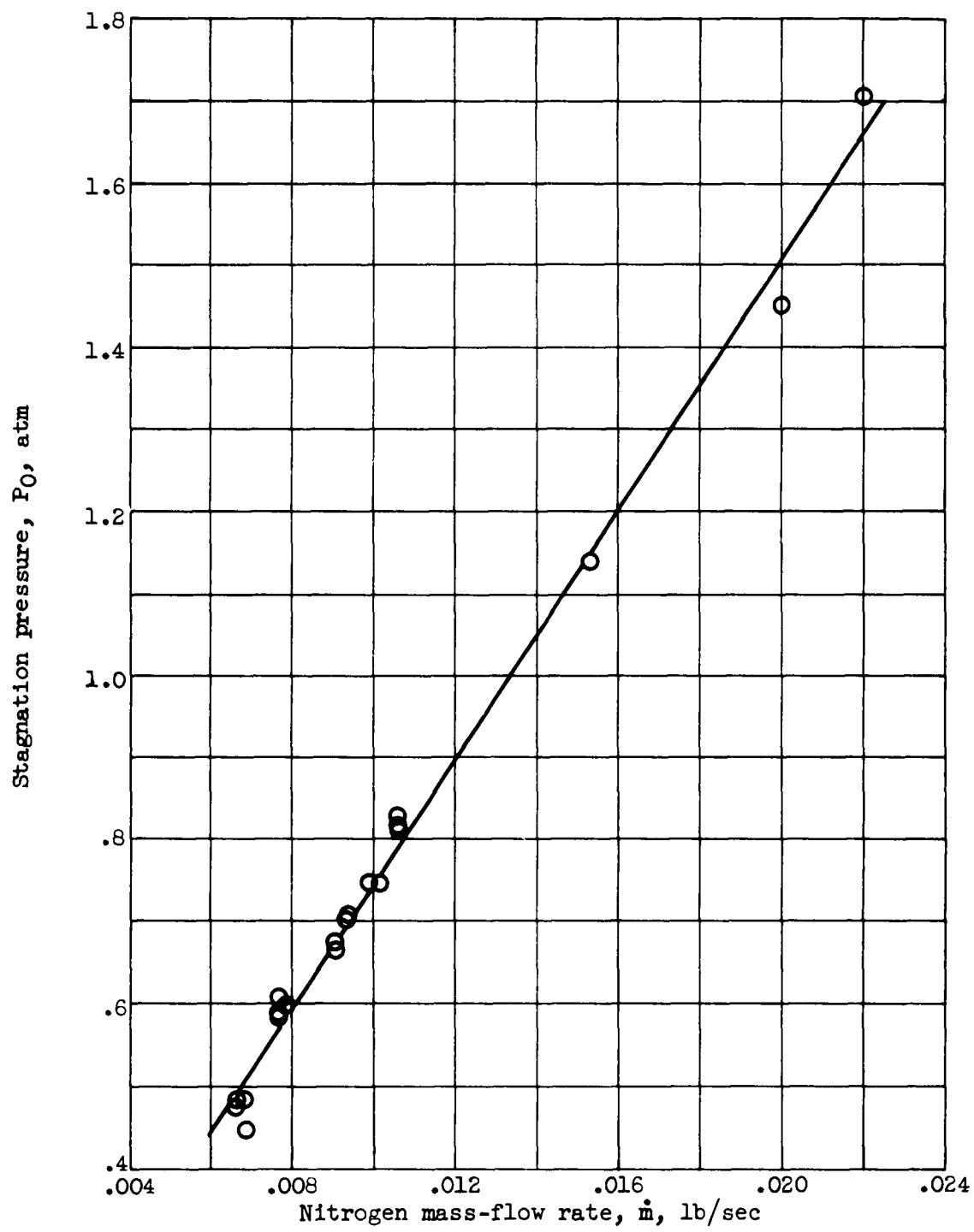


Figure 12. - Variation of stagnation pressure with nitrogen mass-flow rate for triple-cathode electrode configuration using 0.5-inch-throat-diameter nozzle. Ballast resistor, 0.16 ohm in series with each cathode plus 0.07 ohm in common; stagnation enthalpy, 5500 to 8100 Btu per pound.

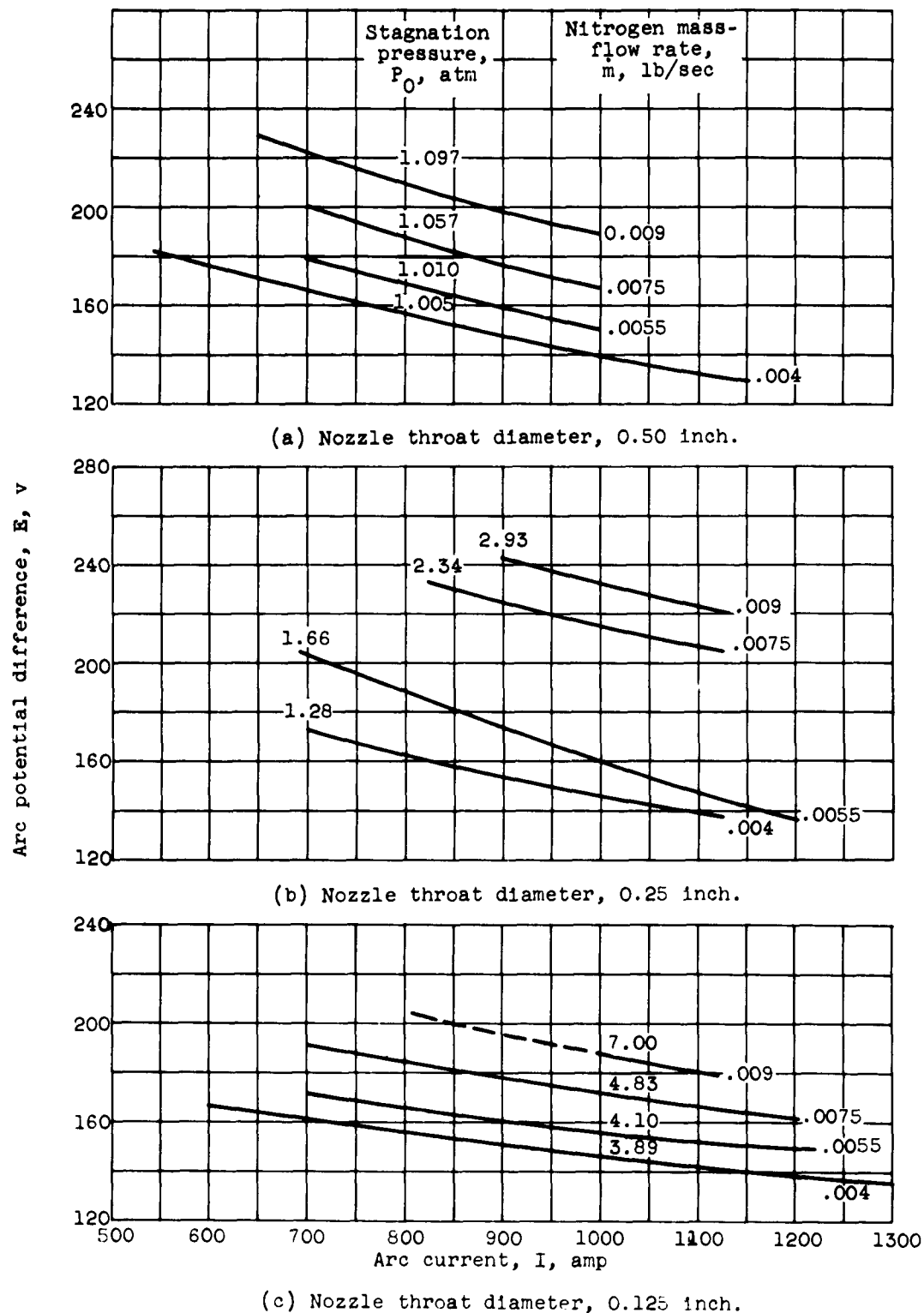


Figure 13. - Smoothed arc potential characteristic curves for single-cathode electrode configuration operating in nitrogen and using 0.32-ohm ballast resistor.

E-1385

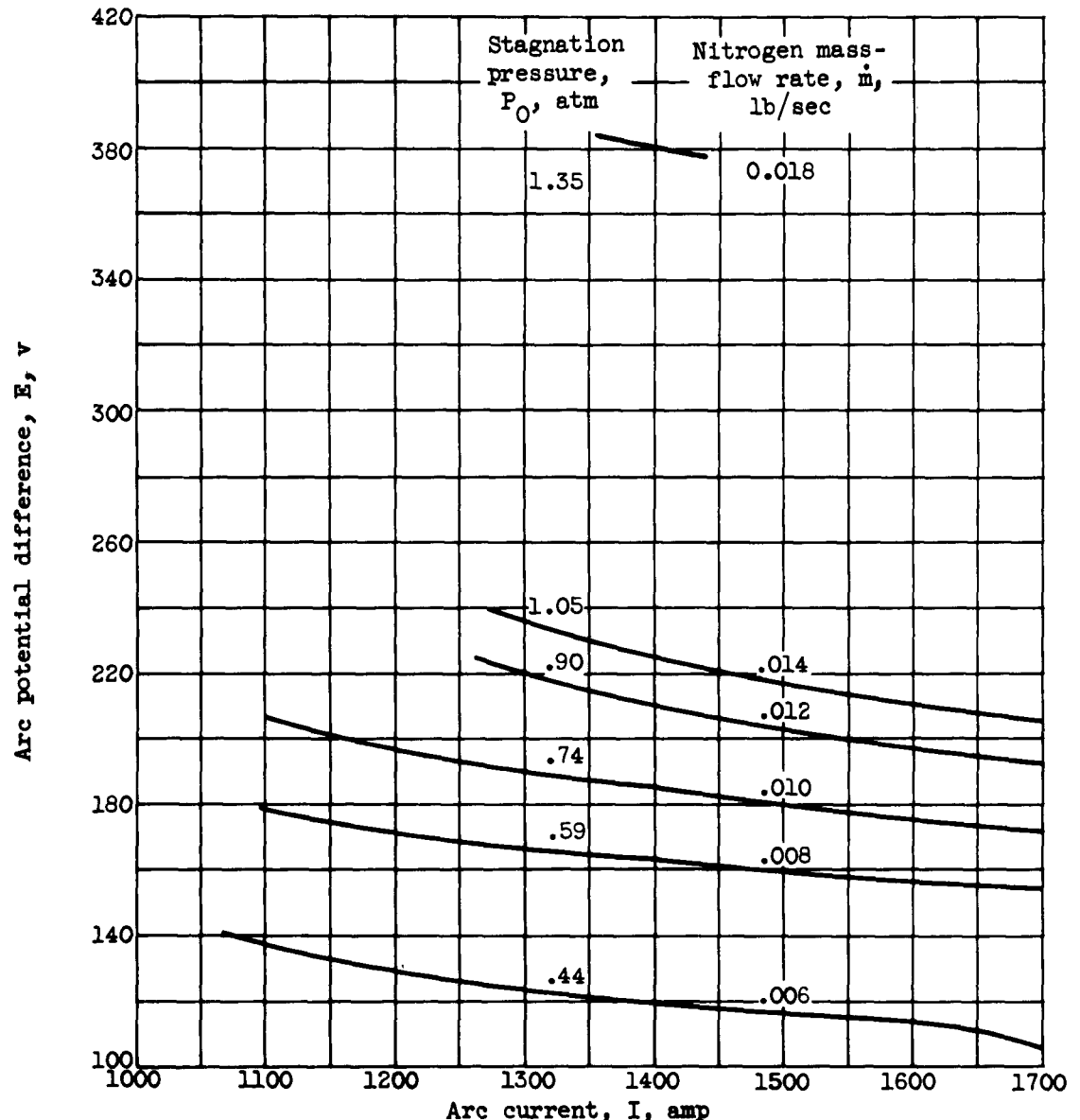


Figure 14. - Smoothed arc potential characteristic curves for triple-cathode electrode configuration operating in nitrogen using 0.5-inch-throat-diameter nozzle.

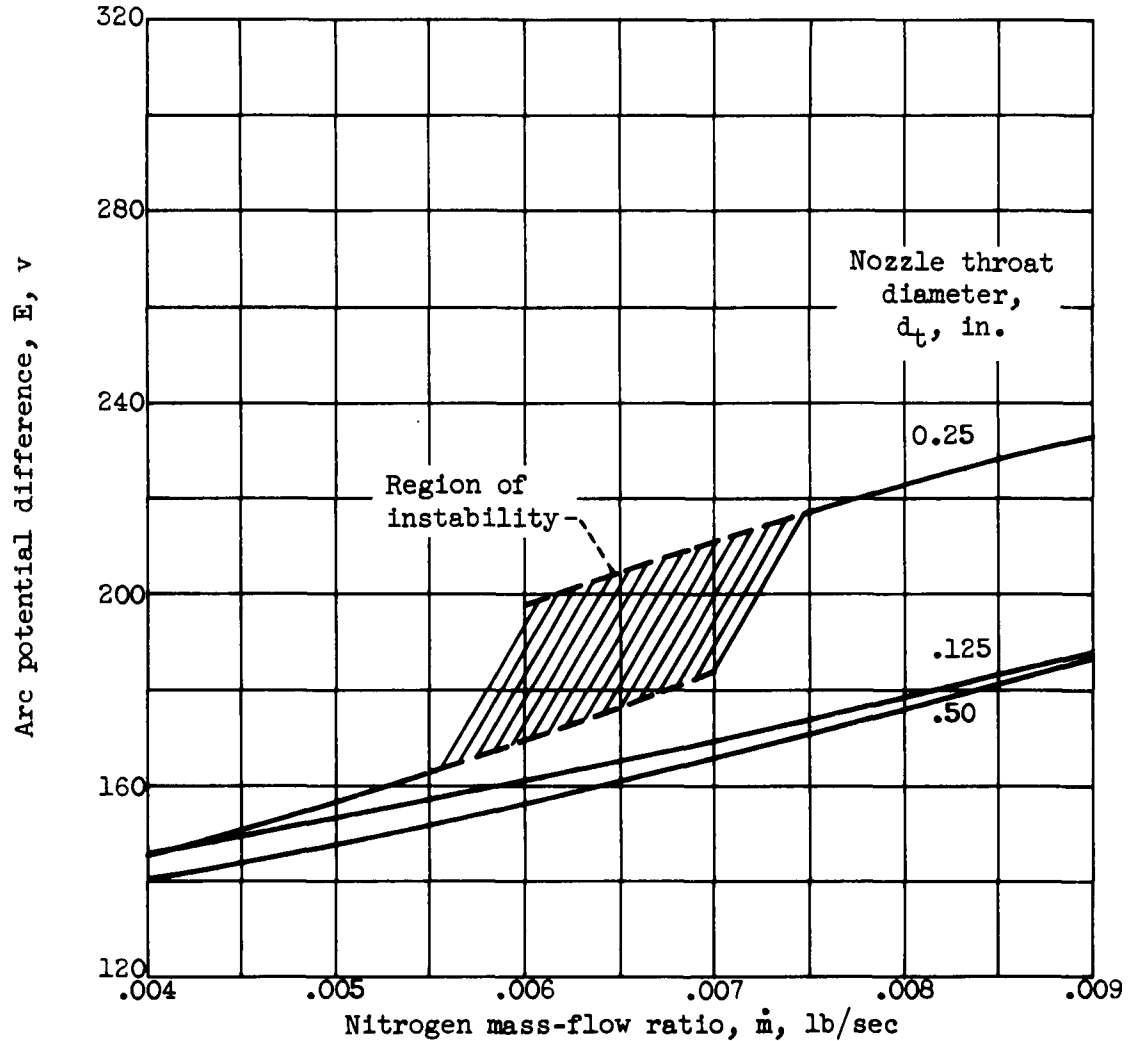
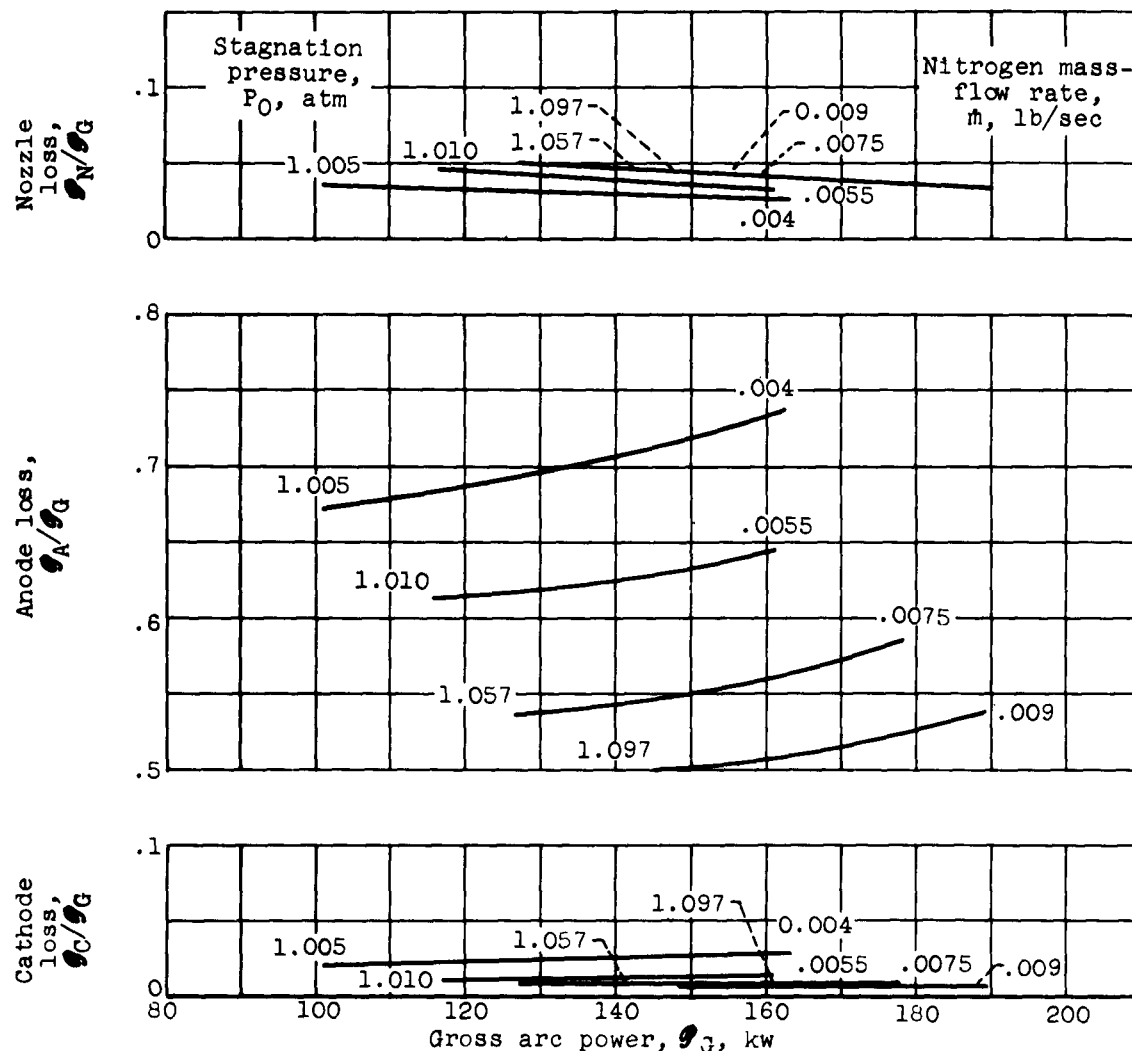


Figure 15. - Variation of arc potential with nitrogen mass-flow rate for single-cathode electrode configuration incorporating 0.32-ohm ballast resistor and operating at current of 1000 amperes.

E-1385



(a) Nozzle throat diameter, 0.50 inch.

Figure 16. - Variation of component losses with gross power and nitrogen mass-flow rate for single-cathode electrode configuration using 0.32-ohm ballast resistor.

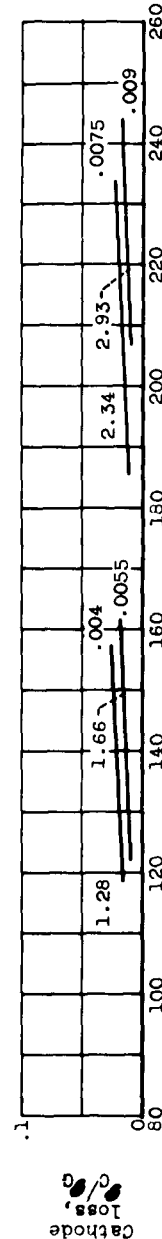
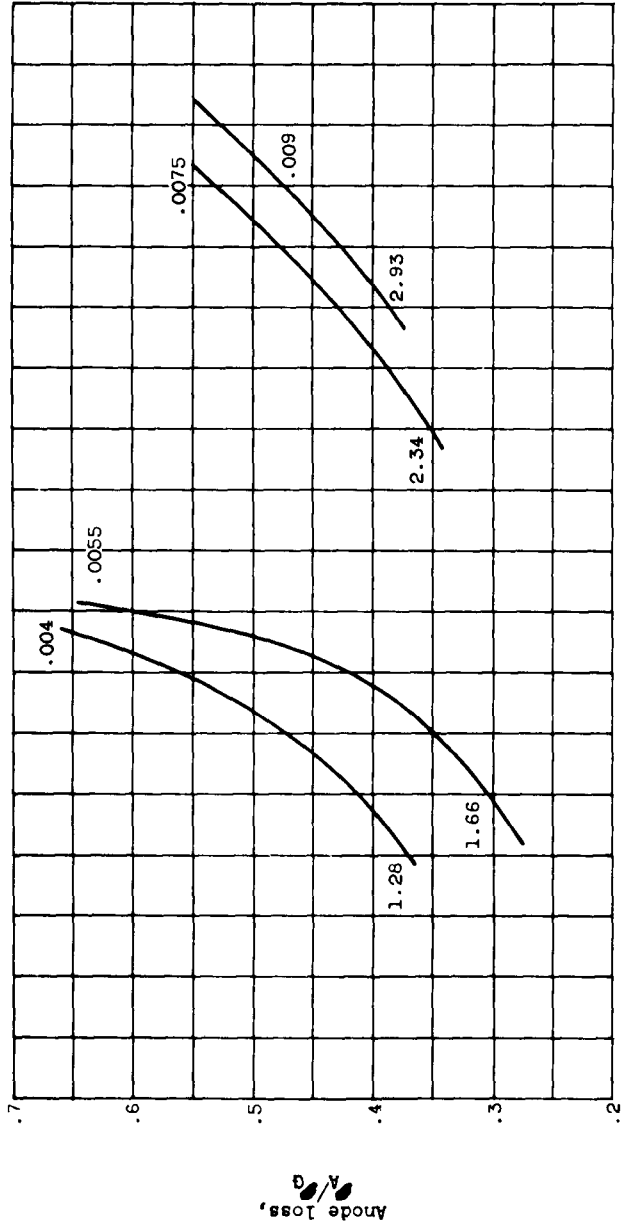
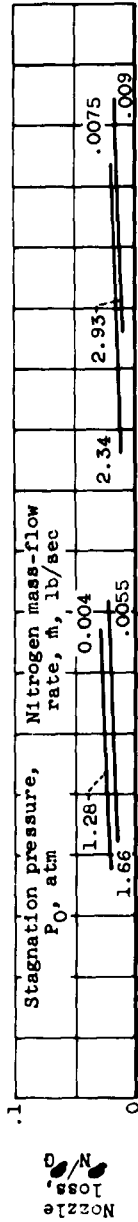
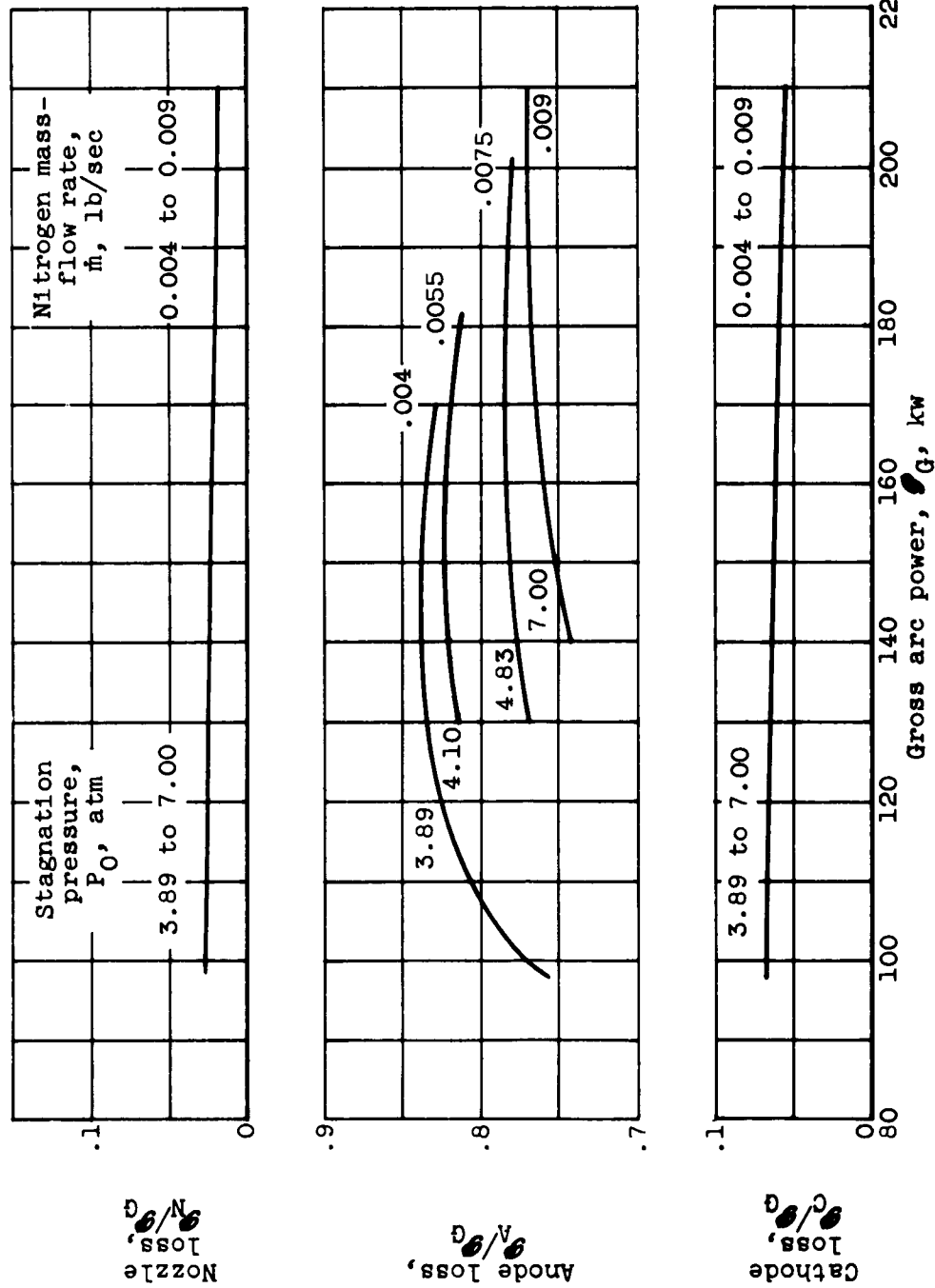


Figure 16. - Continued. Variation of component losses with gross power and nitrogen mass-flow rate for single-cathode electrode configuration using 0.32-ohm ballast resistor.

(b) Nozzle throat diameter, 0.25 inch.

E-1385



(c) Nozzle throat diameter, 0.125 inch.

Figure 16. - Concluded. Variation of component losses with gross power and nitrogen mass-flow rate for single-cathode electrode configuration using 0.32-ohm ballast resistor.

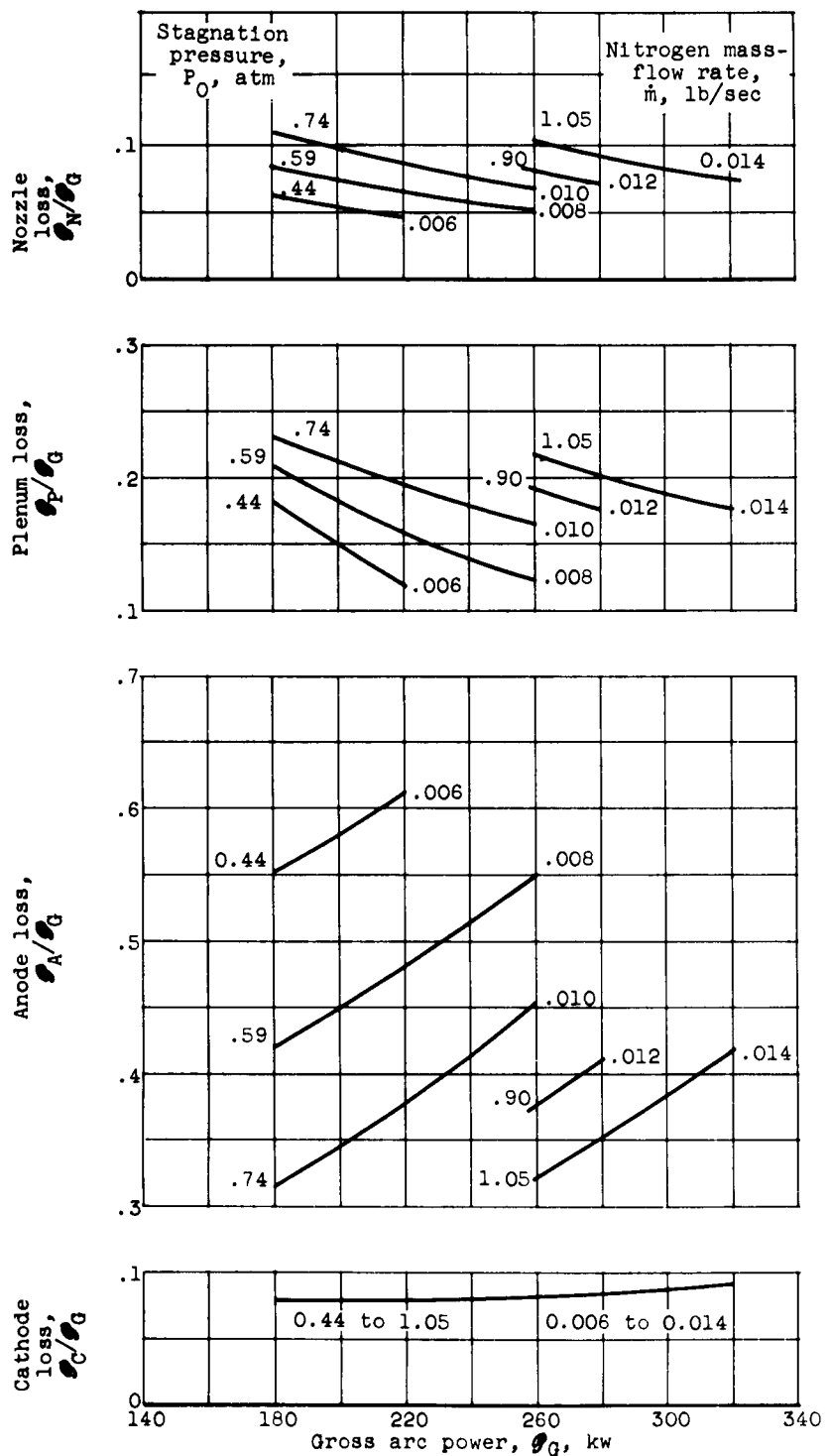


Figure 17. - Smoothed curves indicating variation of component losses with gross power and nitrogen mass-flow rate for triple-cathode electrode configuration and 0.5-inch-throat-diameter nozzle. Ballast resistor, 0.16 ohm in series with each cathode plus 0.07 ohm in common.

E-1385

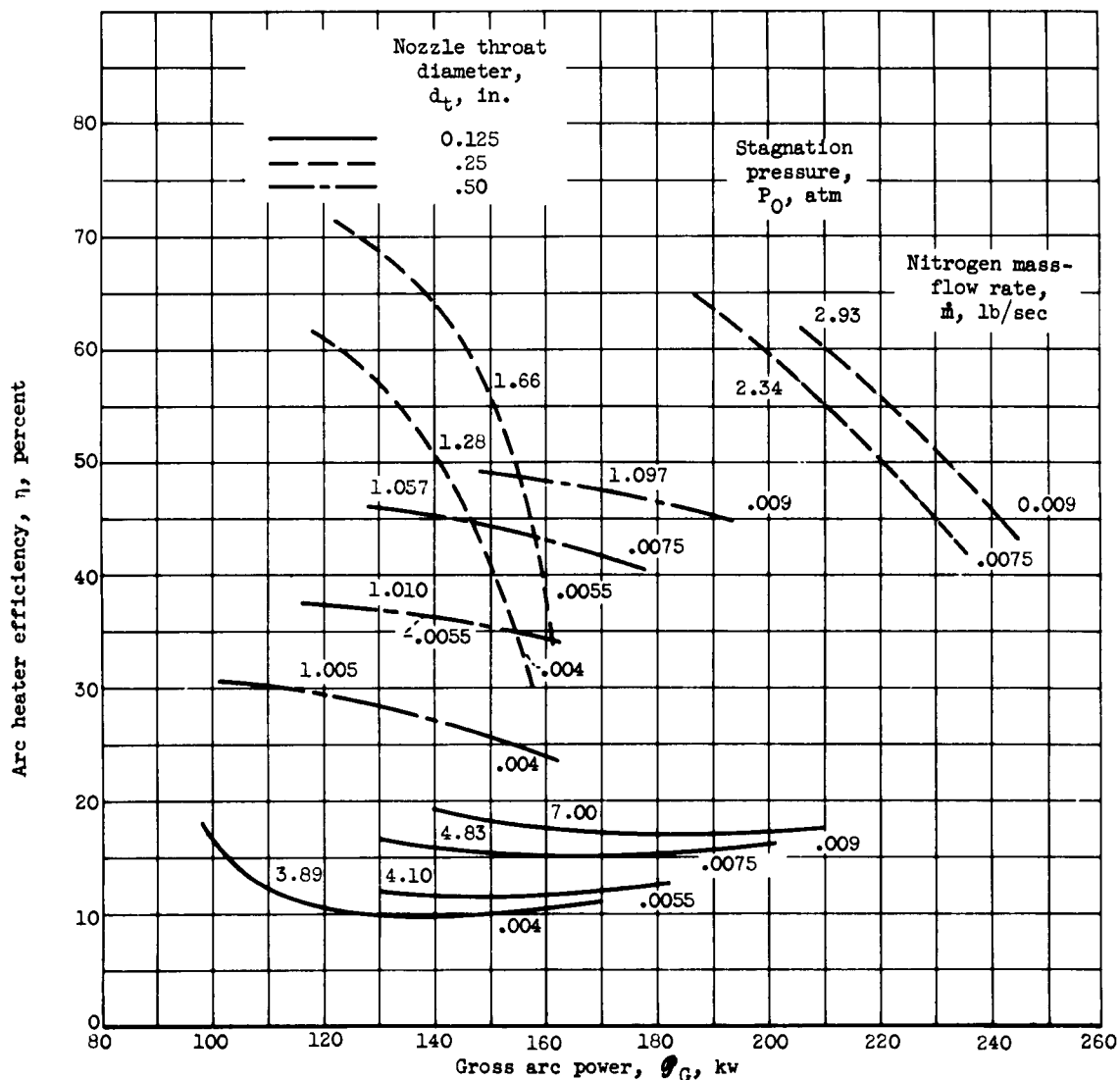


Figure 18. - Smoothed curves indicating variation of arc heater efficiency with gross power and nitrogen mass-flow rate for single-cathode electrode configuration using 0.32-ohm ballast resistor.

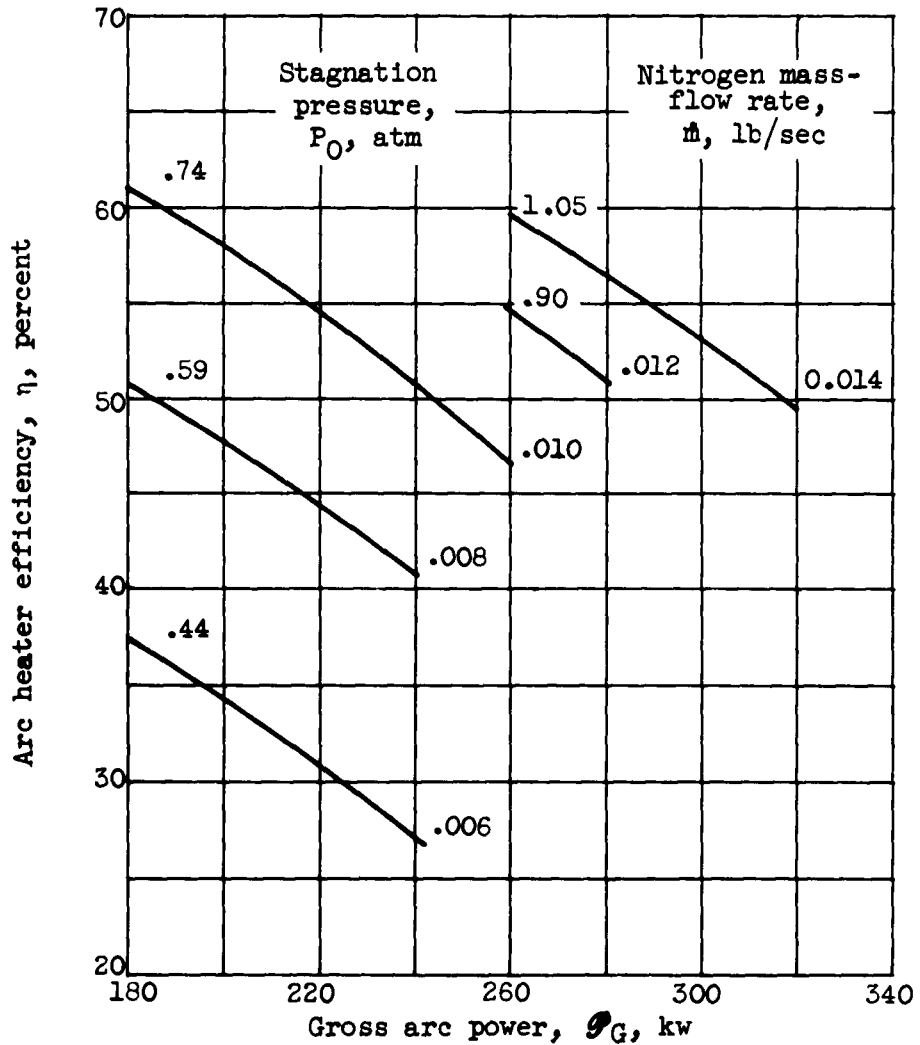


Figure 19. - Smoothed curves indicating variation of arc heater efficiency with gross power and nitrogen mass-flow rate for triple-cathode electrode configuration using 0.5-inch-throat-diameter nozzle. Ballast resistor, 0.016 ohm in series with each cathode plus 0.07 ohm in common.

E-1385

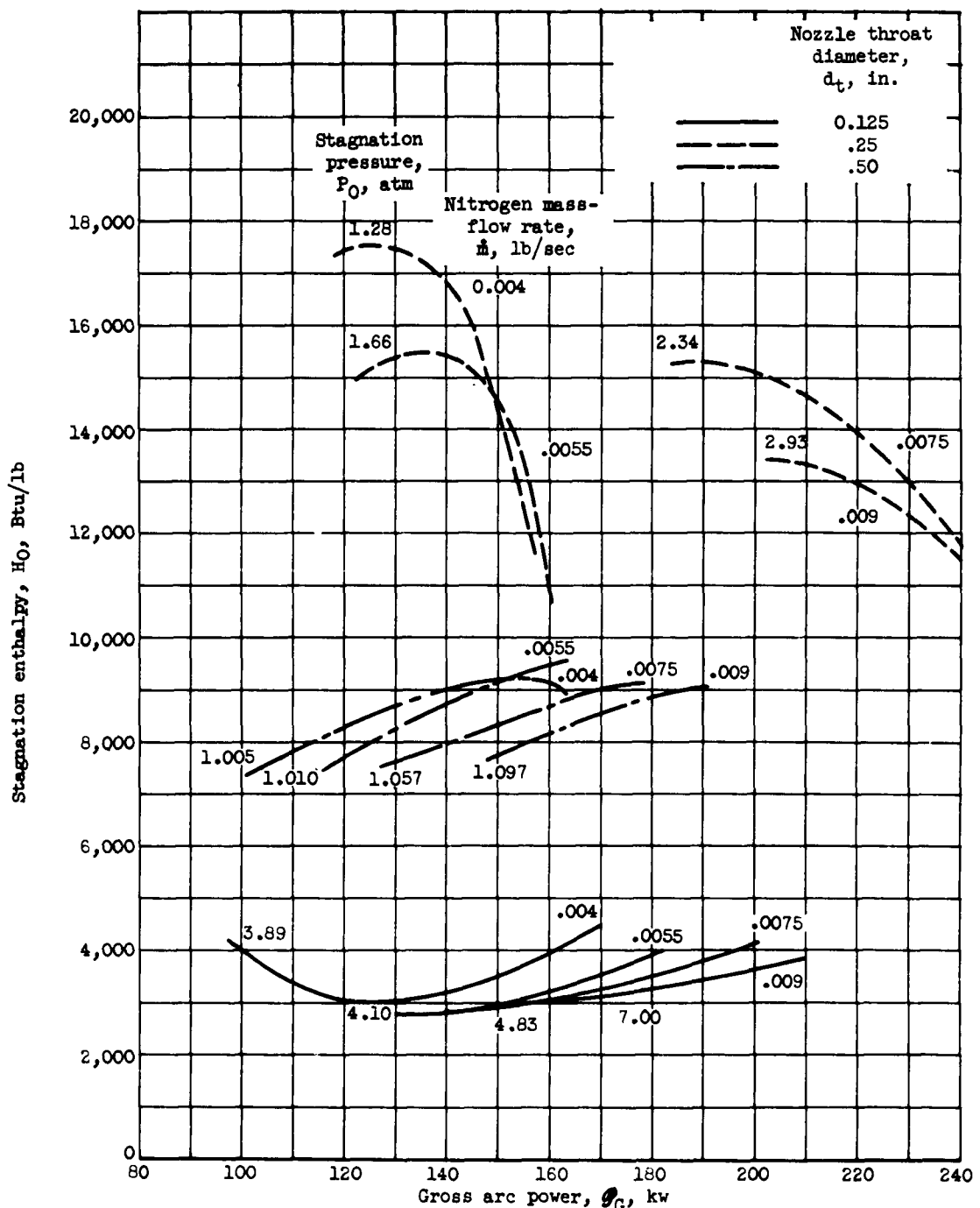


Figure 20. - Smoothed curves indicating variation of stagnation enthalpy with gross power and nitrogen mass-flow rate for single-cathode electrode configuration using 0.32-ohm ballast resistor.

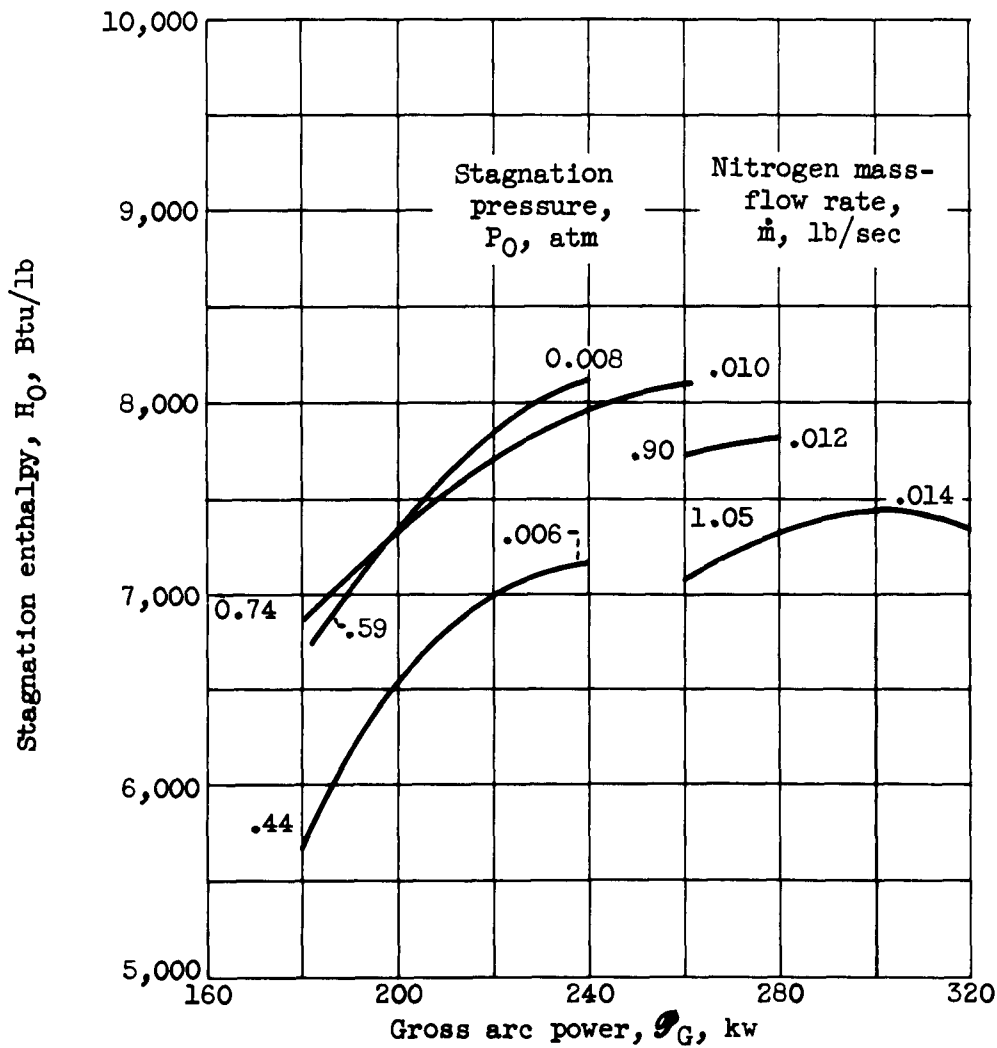


Figure 21. - Smoothed curves indicating variation of stagnation enthalpy with gross power and nitrogen mass-flow rate for triple-cathode electrode configuration using 0.5-inch-throat-diameter nozzle.  
Ballast resistor, 0.16 ohm in series with each cathode plus 0.07 ohm in common.

E-1385

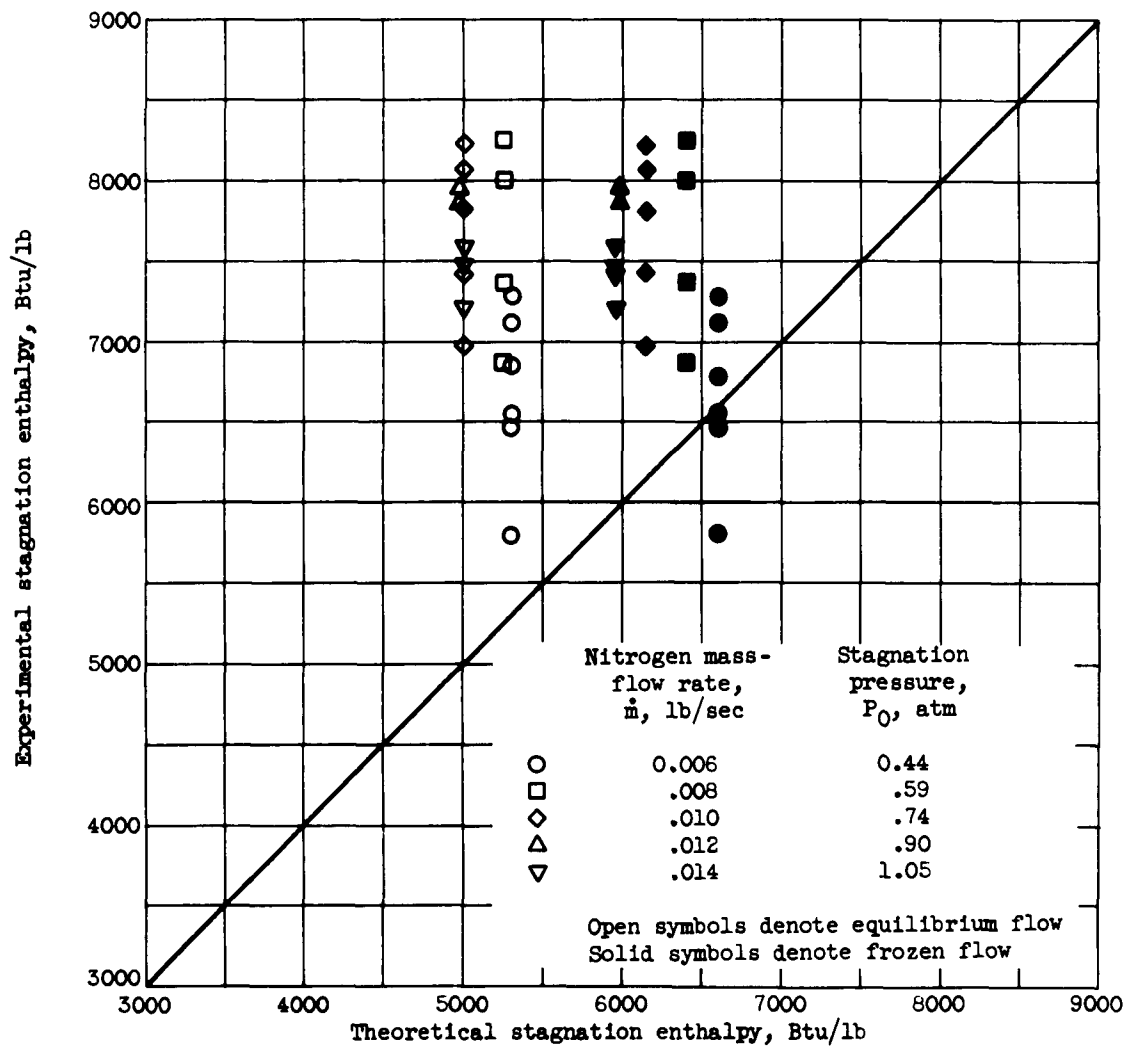


Figure 22. - Comparison of experimental (energy balance) stagnation enthalpy for nitrogen with theoretical values based on equilibrium and frozen critical air-flow for triple-cathode configuration using 0.5-inch-throat-diameter nozzle.

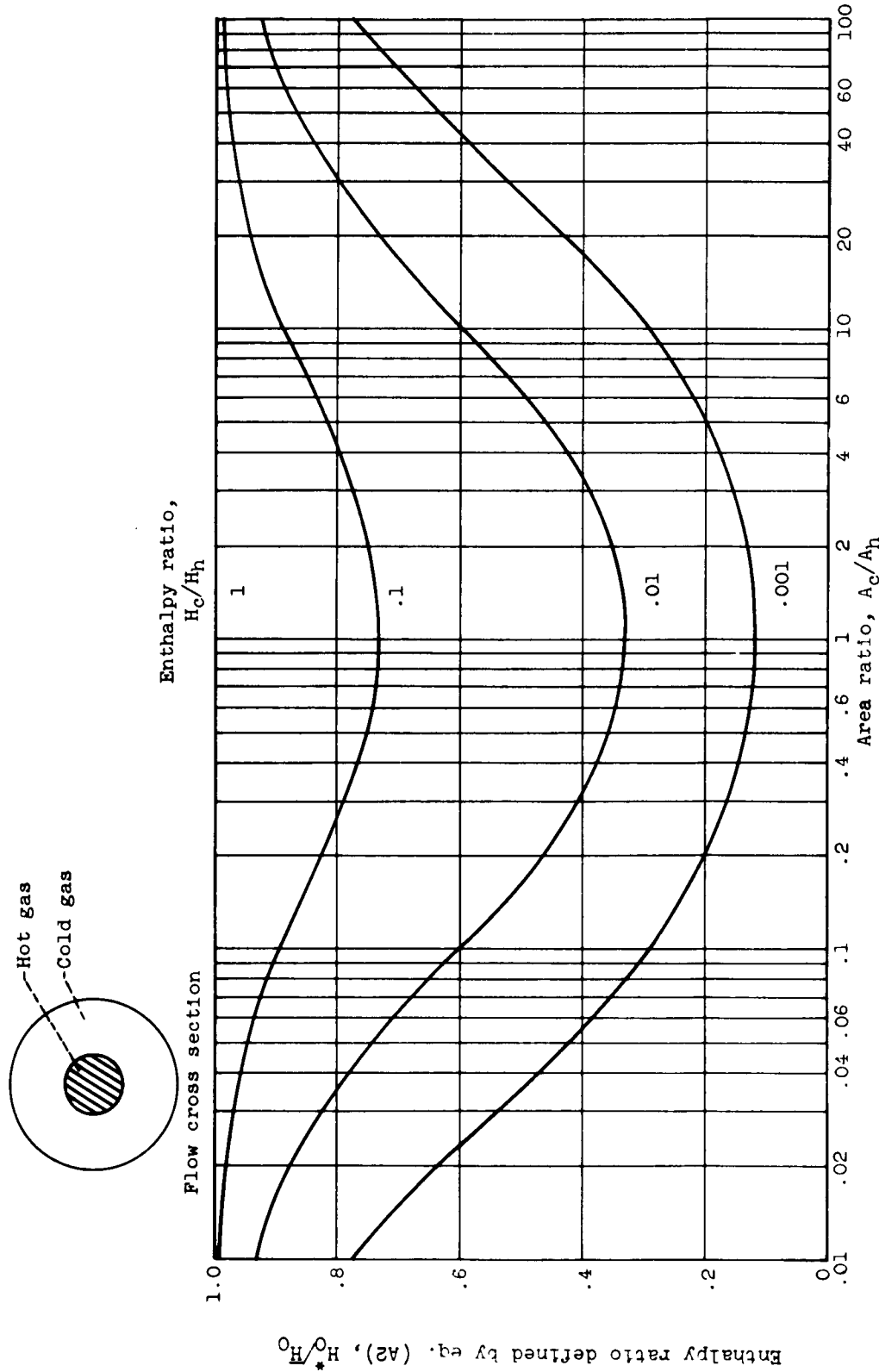


Figure 23. - Perfect gas comparison of effect of nonuniform enthalpy profile on theoretical average stagnation enthalpy.

E-1385

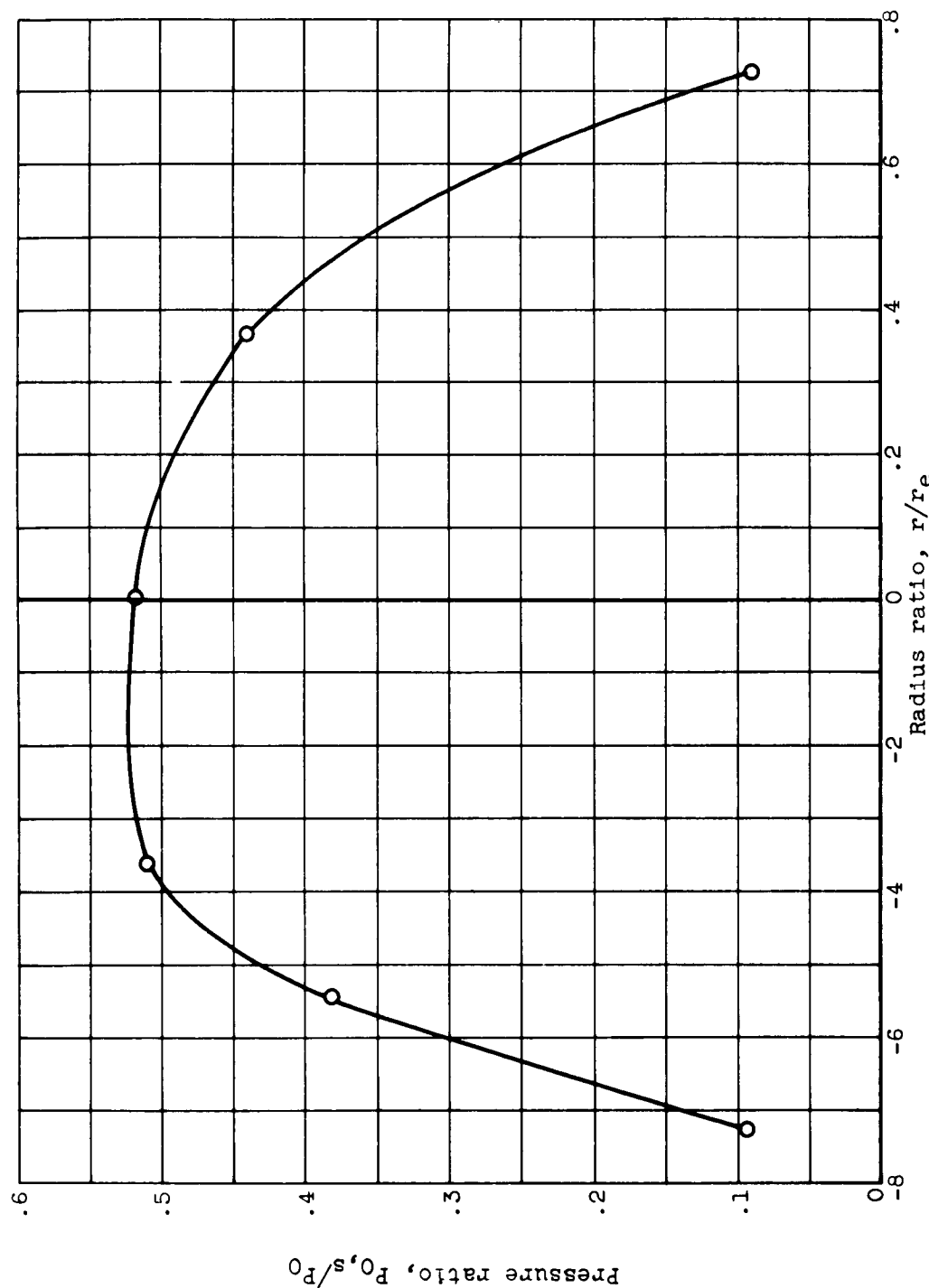


Figure 24. - Nozzle exit total-pressure profile for triple-cathode electrode configuration. Nitrogen mass-flow rate, 0.0093 pound per second; stagnation pressure, 0.709 atmosphere; nozzle throat diameter, 0.5 inch; nozzle exit radius, 0.69 inch.

NASA TN D-1222  
National Aeronautics and Space Administration.  
ELECTRODE CONFIGURATIONS FOR A WIND-  
TUNNEL HEATER INCORPORATING THE MAGNET-  
ICALLY SPUN ELECTRIC ARC. Donald R. Boldman,  
Charles E. Shepard, and John C. Fakan. April  
1962. 51p. OTS price, \$1.50.  
(NASA TECHNICAL NOTE D-1222)

I. Boldman, Donald R.  
II. Shepard, Charles E.  
III. Fakan, John C.  
IV. NASA TN D-1222  
(Initial NASA distribution:  
20, Fluid mechanics;  
41, Propulsion systems,  
electric;  
45, Research and develop-  
ment facilities.)

Various arc heater configurations incorporating a magnetically spun arc were tested over a range of nitrogen flow rates, power levels, and pressures. An evaluation was conducted for a specific configuration of the aforementioned type in order to determine the independent effect of pressure on arc potential difference, heater efficiency, and stagnation enthalpy. Performance results are also presented for another version of the arc heater in which multiple cathodes were used to produce a higher power. A correlation of the stagnation enthalpy determined by an energy balance with theoretical-equilibrium

Copies obtainable from NASA, Washington  
(over)

NASA

I. Boldman, Donald R.  
II. Shepard, Charles E.  
III. Fakan, John C.  
IV. NASA TN D-1222  
TUNNEL HEATER INCORPORATING THE MAGNET-  
ICALLY SPUN ELECTRIC ARC. Donald R. Boldman,  
Charles E. Shepard, and John C. Fakan. April  
1962. 51p. OTS price, \$1.50.  
(NASA TECHNICAL NOTE D-1222)

I. Boldman, Donald R.  
II. Shepard, Charles E.  
III. Fakan, John C.  
IV. NASA TN D-1222  
(Initial NASA distribution:  
20, Fluid mechanics;  
41, Propulsion systems,  
electric;  
45, Research and develop-  
ment facilities.)

Various arc heater configurations incorporating a magnetically spun arc were tested over a range of nitrogen flow rates, power levels, and pressures. An evaluation was conducted for a specific configuration of the aforementioned type in order to determine the independent effect of pressure on arc potential difference, heater efficiency, and stagnation enthalpy. Performance results are also presented for another version of the arc heater in which multiple cathodes were used to produce a higher power. A correlation of the stagnation enthalpy determined by an energy balance with theoretical-equilibrium

Copies obtainable from NASA, Washington  
(over)

NASA

NASA TN D-1222  
National Aeronautics and Space Administration.  
ELECTRODE CONFIGURATIONS FOR A WIND-  
TUNNEL HEATER INCORPORATING THE MAGNET-  
ICALLY SPUN ELECTRIC ARC. Donald R. Boldman,  
Charles E. Shepard, and John C. Fakan. April  
1962. 51p. OTS price, \$1.50.  
(NASA TECHNICAL NOTE D-1222)

I. Boldman, Donald R.  
II. Shepard, Charles E.  
III. Fakan, John C.  
IV. NASA TN D-1222  
(Initial NASA distribution:  
20, Fluid mechanics;  
41, Propulsion systems,  
electric;  
45, Research and develop-  
ment facilities.)

Various arc heater configurations incorporating a magnetically spun arc were tested over a range of nitrogen flow rates, power levels, and pressures. An evaluation was conducted for a specific configuration of the aforementioned type in order to determine the independent effect of pressure on arc potential difference, heater efficiency, and stagnation enthalpy. Performance results are also presented for another version of the arc heater in which multiple cathodes were used to produce a higher power. A correlation of the stagnation enthalpy determined by an energy balance with theoretical-equilibrium

Copies obtainable from NASA, Washington  
(over)

NASA

I. Boldman, Donald R.  
II. Shepard, Charles E.  
III. Fakan, John C.  
IV. NASA TN D-1222  
TUNNEL HEATER INCORPORATING THE MAGNET-  
ICALLY SPUN ELECTRIC ARC. Donald R. Boldman,  
Charles E. Shepard, and John C. Fakan. April  
1962. 51p. OTS price, \$1.50.  
(NASA TECHNICAL NOTE D-1222)

I. Boldman, Donald R.  
II. Shepard, Charles E.  
III. Fakan, John C.  
IV. NASA TN D-1222  
(Initial NASA distribution:  
20, Fluid mechanics;  
41, Propulsion systems,  
electric;  
45, Research and develop-  
ment facilities.)

Various arc heater configurations incorporating a magnetically spun arc were tested over a range of nitrogen flow rates, power levels, and pressures. An evaluation was conducted for a specific configuration of the aforementioned type in order to determine the independent effect of pressure on arc potential difference, heater efficiency, and stagnation enthalpy. Performance results are also presented for another version of the arc heater in which multiple cathodes were used to produce a higher power. A correlation of the stagnation enthalpy determined by an energy balance with theoretical-equilibrium

Copies obtainable from NASA, Washington  
(over)

NASA

Copies obtainable from NASA, Washington  
(over)

NASA

NASA TN D-1222

and frozen-critical-flow values resulted in poor  
agreement primarily because little was known about  
the actual flow process.

NASA TN D-1222

and frozen-critical-flow values resulted in poor  
agreement primarily because little was known about  
the actual flow process.

Copies obtainable from NASA, Washington

NASA

Copies obtainable from NASA, Washington

NASA

NASA TN D-1222

and frozen-critical-flow values resulted in poor  
agreement primarily because little was known about  
the actual flow process.

NASA TN D-1222

and frozen-critical-flow values resulted in poor  
agreement primarily because little was known about  
the actual flow process.

Copies obtainable from NASA, Washington

NASA

Copies obtainable from NASA, Washington

NASA